

Article

Smooth DNA Transport through a Narrowed Pore Geometry

Spencer Carson,¹ James Wilson,² Aleksei Aksimentiev,² and Meni Wanunu^{1,3,*}¹Department of Physics, Northeastern University, Boston, Massachusetts; ²Department of Physics, University of Illinois at Urbana-Champaign, Urbana, Illinois; and ³Department of Chemistry and Chemical Biology, Northeastern University, Boston, Massachusetts

ABSTRACT Voltage-driven transport of double-stranded DNA through nanoscale pores holds much potential for applications in quantitative molecular biology and biotechnology, yet the microscopic details of translocation have proven to be challenging to decipher. Earlier experiments showed strong dependence of transport kinetics on pore size: fast regular transport in large pores (> 5 nm diameter), and slower yet heterogeneous transport time distributions in sub-5 nm pores, which imply a large positional uncertainty of the DNA in the pore as a function of the translocation time. In this work, we show that this anomalous transport is a result of DNA self-interaction, a phenomenon that is strictly pore-diameter dependent. We identify a regime in which DNA transport is regular, producing narrow and well-behaved dwell-time distributions that fit a simple drift-diffusion theory. Furthermore, a systematic study of the dependence of dwell time on DNA length reveals a single power-law scaling of 1.37 in the range of 35–20,000 bp. We highlight the resolution of our nanopore device by discriminating via single pulses 100 and 500 bp fragments in a mixture with >98% accuracy. When coupled to an appropriate sequence labeling method, our observation of smooth DNA translocation can pave the way for high-resolution DNA mapping and sizing applications in genomics.

INTRODUCTION

Cellular DNA is generally found in the nucleus in the form of a long double-stranded DNA (dsDNA) helix. During transcription and other DNA metabolic processes, specialized proteins can slide along the DNA contour in search of a specific sequence, chemical modifications, or chemical damage. Recently, nanopores in synthetic materials and engineered protein channels have emerged as single-molecule tools for similarly identifying sequence and other structural features along DNA contours (1–5). In this method, DNA molecules are electrophoretically pulled into an electrolyte-filled nanopore by applying a small voltage bias (< 0.5 V) across it. DNA entry and passage through the pore are detected by monitoring the ion current signal across the pore. Temporal fluctuations in the signal can report on the presence of epigenetic modifications (6–10), alteration in sequence (11–15), length variation (16,17), secondary structure (17,18), and conformation (19–21) of the DNA molecule. Prospects for nanopores as DNA sequence scanners, high-resolution DNA sequence mappers, and epigenetic modification detectors have fueled research that aims to understand the details of DNA translocation and its limitations. In comparison to existing technologies, scanning DNA fragments at high-throughput is potentially more attractive than optical DNA stretching methods (22–24) because 1) electronic measurement devices can be more easily miniaturized; 2) electronic measurements can be made at MHz bandwidths, allowing faster processes to be

probed, i.e., higher throughput; and 3) the resolution of nanopore measurements is ideally dictated by its geometry (2–5 nm), whereas optical methods are constrained by undesirable photophysical features of dye molecules and optical diffraction limits (~100s of nm).

Despite ample promise, two major shortcomings of nanopores with respect to dsDNA analysis have been 1) Mean transport speeds are 10–100 times faster than required for statistical averaging of ion current data from short DNA regions inside the pore (5), and 2) DNA position versus time in the pore is not well known or otherwise regulated (3,25,26). Although regulation has been achieved for single-stranded DNA using enzymes as molecular stepper motors (9,10,27–31), regulated motion of dsDNA has yet to be demonstrated. Voltage-driven dsDNA translocation through 5–15 nm diameter pores in thin (20–50 nm) solid-state materials proceeds with mean velocities of 10–100 ns/bp, and often in large pores multiple DNA strands enter simultaneously (17,19,32,33), which complicates single-file readout of information that is encoded in the linear sequence. Proteins such as RecA from *Escherichia coli* form filaments around the DNA that slows DNA transport and prevents its folding (26,34,35), although this approach inherently masks chemical information contained within the DNA, such as the presence of DNA chemical modifications (7,36) or small bound drug/reporter molecules (37–40). Explorations of the effects of parameters such as the electrolyte viscosity (41,42), salt type (43,44), membrane material (45,46), applied pressure (47,48), and chemical composition inside (49–52) and outside (53) the pore have yielded only moderate DNA retardation factors.

Submitted August 22, 2014, and accepted for publication October 15, 2014.

*Correspondence: wanunu@neu.edu

Editor: Hagan Bayley.

© 2014 by the Biophysical Society
0006-3495/14/11/2381/13 \$2.00



In contrast, the use of smaller diameter pores (< 5 nm) results in mean DNA velocities that are reduced easily by ~ 2 orders of magnitude (5,54–56) while simultaneously preventing folded DNA transport. However, the statistics of DNA transport times through sub-5 nm pores point to a highly complex process: a pure single-length DNA fragment can produce multiple event populations that are characterized by broad distributions of dwell times and blockade amplitudes (19,55–58). Based on their dependence on various parameters, these distinct subpopulations have been associated with various processes such as nontransport DNA collisions with the pore and translocation governed by strong interactions. Despite this, the broad and overlapping nature of these subpopulations is a grand impediment of DNA mapping applications as it implies a greatly smeared DNA positional trajectory during translocation.

In this work we present a systematic study that pinpoints and overcomes the source for irregular DNA transport through small pores. Our findings have led us to conclude that the anomalous transport dynamics is related to electric field-driven DNA self-interaction between extra-pore and intrapore segments. Furthermore, these interactions are efficiently extinguished by restricting the pore diameter, leading to reproducible transport time distributions with unprecedentedly low scatter. Molecular dynamics (MD) simulations of DNA diffusion within the pore constraint and quantitative fits of our statistical data to a one-dimensional (1D) Fokker-Planck model support a greatly reduced DNA axial diffusion in sub-3 nm diameter pores. This explains the favorably slow DNA velocities and the low scatter in DNA velocities for a given experiment. Mean transport times are related to DNA length in the range of 35–20,000 bp through a single superlinear power law, which in combination with prior studies appears to be weakly related to pore diameter. Finally, we demonstrate DNA fragment length discrimination in a mixture from a single pulse with $>98\%$ accuracy.

MATERIALS AND METHODS

Nanopore experiments

For all details about nanopore fabrication and information about our experimental setup, please refer to section SM-1 in the [Supporting Material](#). Unless otherwise indicated, all experiments were performed at room temperature (25°C) and using 0.40 M KCl electrolyte tris-buffered to pH 7.9.

Data acquisition and analysis

Experimental data were collected using the Chimera Instruments VC100 (New York, NY) at a sampling rate of 4.19 MHz, and further digitally low-pass filtered at 200 kHz before analysis to reduce the capacitance noise. The high-bandwidth increases our time resolution and ensures that events as fast as 2.5 μ s are detected. All DNA samples used in these studies were obtained from Thermo Scientific (Waltham, MA). Analysis of all nanopore data was performed using MATLAB-based OpenNanopore software (59)

developed by the Radenovic group at Ecole Polytechnique Fédérale de Lausanne (EPFL), which uses a cumulative sums algorithm to detect individual events in the raw current signals. Standard errors shown for D and v were estimated using a bootstrapping procedure that is described thoroughly in the [Supporting Material SM-1](#).

MD simulations of diffusion in pore-confined DNA

MD simulations were performed using the NAMD (60) software package. Periodic boundary conditions were applied, and particle mesh Ewald electrostatics (61) governed the long-range interactions. Multiple time stepping (62) was used so that local interactions were calculated every time step, and the full electrostatic calculation was performed every 3 time steps. A 2 fs time step was used with RATTLE (63) and SETTLE (64) algorithms applied to covalent bonds involving hydrogens in DNA and water, respectively. The van der Waals forces were smoothly cutoff starting at 7 Å and were completely cutoff at 8 Å. The CHARMM36 (65) force field was used for nucleic acids, water, and ions, with NBFIX corrections for ions (66), and a custom force field for Si_3N_4 (67). The NPT simulations used a Nose-Hoover Langevin piston pressure control (68), and the temperature was controlled by a Langevin thermostat acting on the membrane atoms with a damping constant of 1.0 ps^{-1} . During NPT simulations, the DNA and Si_3N_4 were harmonically restrained with a spring constant of 695 $\text{pN}/\text{Å}$. In all NVT production simulations, the surface atoms of the membrane were harmonically restrained with a spring constant of 695 $\text{pN}/\text{Å}$, and the interior atoms of the membrane were harmonically restrained with a spring constant of 69.5 $\text{pN}/\text{Å}$.

Atomic-scale models of silicon nitride nanopores were built following a previously described protocol (20). The pores were made by removing atoms from a crystalline silicon nitride membrane. A 36 bp fragment of dsDNA was introduced into the pore, with its axis collinear with the pore axis. Each DNA/nanopore system was solvated; potassium and chloride ions were added to produce electrically neutral systems of target KCl concentration (1 or 0.40 M). Each system ($\sim 120,000$ atoms) underwent 1000 steps of energy minimization, followed by 1 ns equilibration in the constant area, pressure (1 bar) and temperature (295 K) ensemble maintained using a Langevin piston. All production simulations were carried out in a constant volume/temperature ensemble. For information on the script detailing the pulling of DNA molecules see the [Supporting Material SM-1](#).

Finite element simulations

All simulations presented were computed using COMSOL Multiphysics 4.3b (Burlington, MA) with custom geometries (see the [Supporting Material SM-7](#) for more information).

RESULTS AND DISCUSSION

Fig. 1 a illustrates a molecular model of ~ 150 bp dsDNA fragment being voltage-driven through an ultrathin pore with a diameter of $d \sim 3$ nm. The length of dsDNA shown is one persistence length, intentionally chosen to illustrate the stiff nature of the polymer with respect to the pore dimensions. DNA introduction into the *cis* (*top*) chamber and application of positive bias to the *trans* (*bottom*) chamber results in capture and electrophoresis of individual DNA molecules across the pore. Transport of a DNA molecule produces a transient downward spike in the electrical signal, a result of the temporary restriction in ion flux through the pore. In **Fig. 1 b** we show two continuous traces obtained when 60 nM of 500 bp DNA was added to the *cis* chamber

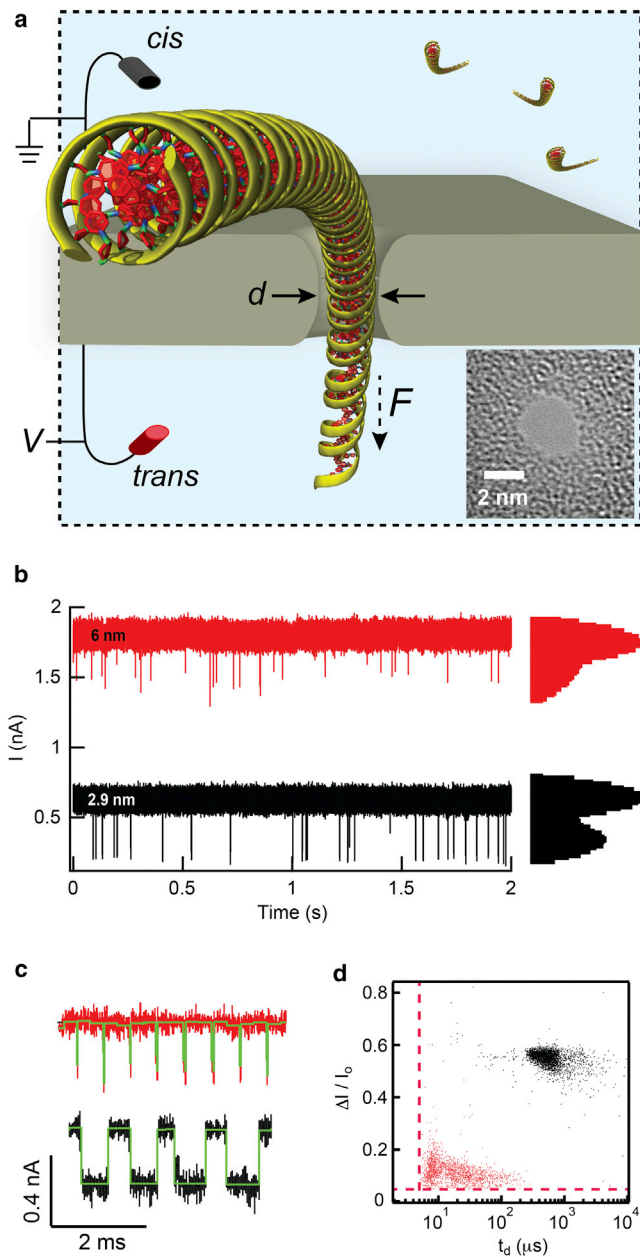


FIGURE 1 Single-molecule DNA electrophoresis. (a) Schematic of ~ 150 bp DNA fragment threading a $d \sim 3$ nm pore (electrodes not to scale), and transmission electron microscopy image of a typical SiN_x nanopore used in experiments. (b) Continuous current versus time traces of 2.9 and 6 nm diameter pores when a 60 nM 500 bp dsDNA sample is added to the *cis* chamber ($V = 200$ mV, data low-pass filtered to 200 kHz). Log-scale all-point current histogram shown on the right illustrates two nanopore states, open pore and DNA-threaded pore. (c) Expanded view of sample events for 2.9 and 6 nm pores after analysis (rectangular analysis fits shown in green). (d) Scatter plots of $\Delta I/I_0$ vs. t_d for 500 bp DNA translocation events through a 2.9 nm (black) and 6 nm (red) pore. Red dotted lines indicate the minimum detectable dwell time and fractional current blockade levels, $t_d = 5$ μs and $\Delta I/I_0 = 0.06$, respectively. To see this figure in color, go online.

and driven using a 200 mV voltage through a 2.9 nm pore and a 6 nm pore. The all-point histograms on the right reveal for each pore two predominant current levels, the higher

corresponding to open pore (I_0) levels and the lower corresponding to DNA-occupied levels. Postacquisition analysis of the traces (OpenNanopore, EPFL (59)) identifies the events as rectangular pulses, a sample of which are shown for both pores in Fig. 1 c. Scatter plots of dwell time t_d versus fractional current blockade $\Delta I/I_0$ are displayed in Fig. 1 d, showing a broad population centered at $t_d \sim 25$ μs and $\Delta I/I_0 \sim 0.12$ for the 6 nm pore ($n_{\text{total}} = 1798$), and $t_d \sim 890$ μs and $\Delta I/I_0 \sim 0.56$ for the 2.9 nm pore ($n_{\text{total}} = 2593$). We note that we can only observe dwell times and current blockades larger than our detection limits (dashed red lines in the plot). Furthermore, only when reducing the bandwidth of our signal do we observe DNA collisions with the pore (see Fig. S1), the vast majority of which produce short-lived, low amplitude pulses. The low scatter in DNA transport times in the smaller of the two pores, which in the course of our experiments has been reproduced for different DNA fragments using over 50 pores, has motivated our study to pinpoint the reasons for smooth DNA transport through pores in the $d = 2.8\text{--}3.0$ nm regime (see Fig. S2 and Fig. S3 for information on stability and pore-to-pore reproducibility).

Voltage fine-tunes DNA transport kinetics through small pores

DNA is a uniformly charged polymer, and therefore its transport kinetics is expected to depend on applied bias. We have chosen to conduct our systematic study using 500 bp dsDNA because it is in the rod-to-coil regime, i.e., its 3+ persistence lengths are sufficiently long to frequently adopt 360° loop configurations at equilibrium (j-factor of ~ 10 nM) (69). In Fig. 2 a we present dwell time distributions for 500 bp DNA transport through a 3.0 nm diameter pore in the 200–350 mV voltage range. The dwell time distributions are asymmetric in shape, and are characterized by sharply increasing peaks at early times followed by broader decays at longer times. The distribution shapes were fit to first-passage time distributions obtained from the 1D Fokker-Planck equation (70,71):

$$f(t_d) = b(4\pi Dt_d^3)^{-1/2} \exp\left[-(b - vt_d)^2 / (4Dt_d)\right] \quad (1)$$

where b is the trajectory length of the molecule, D is the diffusion coefficient, and v is the drift velocity. The model of Eq. 1 describes the 1D motion of a particle that starts at the origin ($x = 0$) of a semiinfinite capillary with an absorbing boundary located at $x = b$. Given that the complete contour length L_C of DNA is longer than the pore length b_{eff} , we set the absorbing boundary to be at $b = b_{\text{eff}} + L_C$ (42,71,72). Phenomenological estimates of b_{eff} for each pore were based on I_0 and ΔI values measured during DNA translocation (73,74) (see the Supporting Material SM-4), whereas L_C values were calculated from

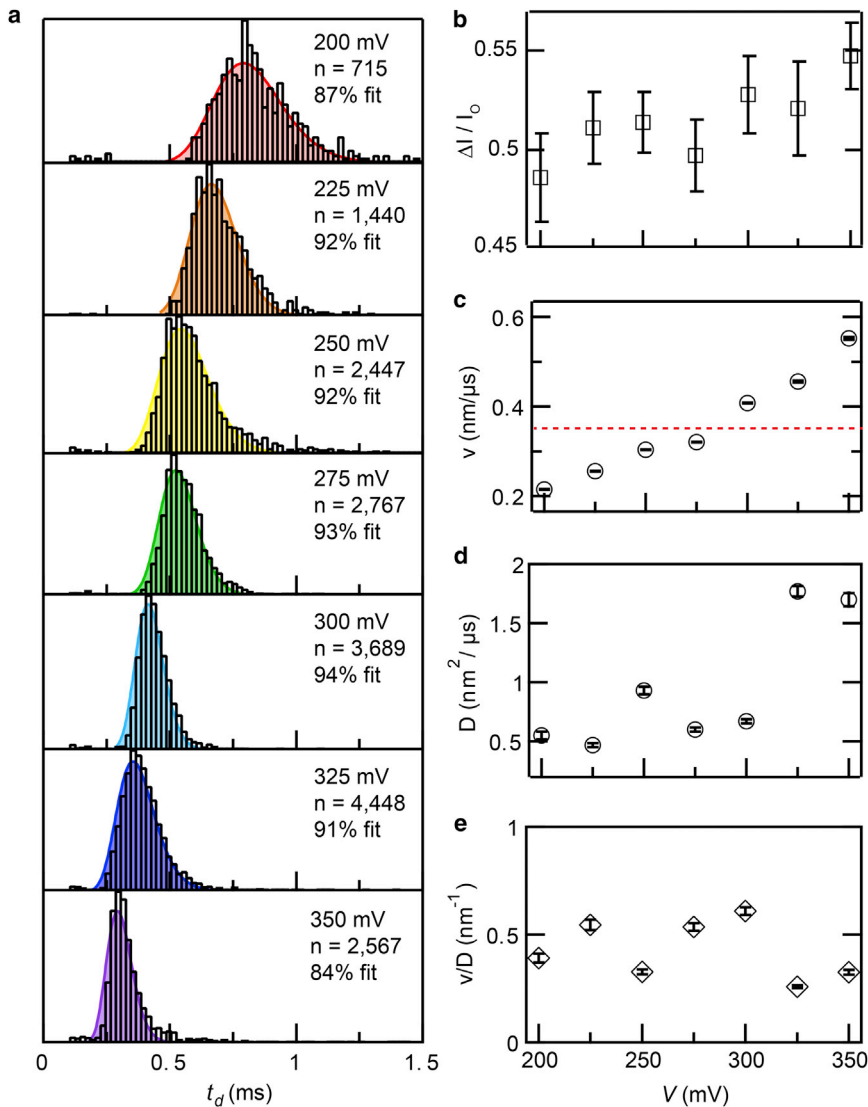


FIGURE 2 Voltage-tuned DNA transport. (a) Dwell time histograms for 500 bp dsDNA transport through a 3.0 nm diameter pore in the 200–350 mV voltage range. Shaded curves represent the optimal fits to the 1D drift-diffusion model of Eq. 1. (b) Fractional current blockade ($\Delta I/I_0$) values as a function of voltage, which remains constant within error throughout the experiment (with the exception of $V = 350$ mV). (c) Values for drift velocity v as a function of voltage, obtained from the fits. In addition to observing very low values for drift velocity, we see that v increases steadily with voltage. A dashed red line is drawn for a value of v corresponding to 1 bp/ μ s. (d) Values for diffusion coefficient D from the fits remain relatively constant for $V \leq 300$ mV, and then increase about threefold for greater V . (e) The quantity of v/D remains remarkably constant throughout the entire voltage range (0.43 ± 0.13 nm⁻¹). To see this figure in color, go online.

$L_C = 0.34N$ nm, where N is the number of basepairs. Best fits to Eq. 1 for each distribution are shown in Fig. 2 a (shaded curves). The percentages of events that fit the model in Eq. 1 lie in the range 84–94% (see the Supporting Material SM-5), where the remaining events outside of the fit are mostly scattered at longer dwell times.

In Fig. 2 b we plot the fractional current blockade ($\Delta I/I_0$) as a function of voltage. We observe a moderate increase in $\Delta I/I_0$ with increasing voltage (6% change from 200 to 350 mV), an effect that was observed in a recent study by the Hall group (58). Drift velocities (v) obtained from the fits are shown in Fig. 2 c. Displayed standard errors for v (and later for D) were calculated by resampling our data for 10,000 iterations using a standard bootstrapping procedure (see Materials and Methods). As previously observed using larger pores (41,75) and for free-solution DNA electrophoresis (76), we find that v increases with voltage. However, v does not depend linearly on voltage and cannot be

extrapolated to the origin, suggesting a voltage-dependent electrophoretic mobility (μ), i.e., $\mu = f(V)$. Mean values of μ obtained in our voltage experiments are on the order of $\sim 10^{-7}$ cm² V⁻¹ s⁻¹, three orders of magnitude smaller than bulk μ values for DNA in free-solution electrophoresis ($\sim 10^{-4}$ cm² V⁻¹ s⁻¹) (77). The obtained values of v yield mean velocities that correspond to one DNA basepair moving through the pore per μ s (dashed red line). We highlight that these are mean values because a constant DNA velocity through a nanopore is unlikely, and further was not proven by this experiment.

The diffusion coefficients (D) of the DNA extracted using Eq. 1 appear to slightly depend on voltage, increasing from 0.5 to 1.8 nm²/ μ s (see Fig. 2 d). A similar trend was recently observed for translocation of stiff fd virus filaments (78). Moreover, as for a rod-like stiff fd filament ($L_C < p$, where p is a persistence length), values for D were comparable to the axial component of their bulk translational diffusion

coefficients. In the case of a semiflexible DNA chain, we argue that a relevant length scale for correlated axial DNA motion is one-half of a persistence length, as opposed to the full DNA contour length. Using reference bulk D_o values for 75 bp ($45 \text{ nm}^2 \mu\text{s}^{-1}$) (79–84), we find that the axial component of D for our experiment is $1.5 D_o$, or $68 \text{ nm}^2/\mu\text{s}$ (see the [Supporting Material SM-6](#) for details). [Fig. 2 d](#) appears to contradict our previous hypothesis, because for all voltages tested we find that D is at least 40 times smaller. In the next section, we will show that the restricted pore geometry is responsible for the greatly reduced D values for DNA, as we recently found for protein electrophoresis in the regime $d_{\text{protein}} \sim d_{\text{pore}}$ (85). Finally, in [Fig. 2 e](#) we show the dependence of the ratio v/D on voltage for this study. Apart from scatter that is mainly a result of the dispersity in measured D values, we find that the ratio v/D is independent of voltage ($0.43 \pm 0.13 \text{ nm}^{-1}$). This suggests that an intricate relationship between v and D governs our observed superlinear dependence of v on voltage, one that is a result of tight molecular confinement and/or interactions within the pore volume.

Impact of pore diameter on DNA translocation

In [Fig. 3](#), *a–e*, we present five representative dwell time distributions for 500 bp DNA transport through 2.6–6 nm diameter pores. Additionally, inset to each distribution we show contour plots of fractional current blockades versus log dwell times, all to the same scale for comparison. First, the inset contour plots reveal a striking 500-fold shift to longer dwell times upon reducing the pore diameter from 6.0 to 2.6 nm ($\sim 10 \mu\text{s}$ to $\sim 5 \text{ ms}$, respectively). In addition

to the longer observed dwell times with decreased pore diameters, their relative scatter (i.e., $\langle t_d \rangle / \sigma_{t_d}$) decrease. Furthermore, upon fitting our data to Eq. 1, as shown by the purple shaded curves, we find for the 3.4–6.0 nm pores a secondary population of long-lived dwell times, indicated by red asterisks in the figures. These doubly populated dwell time distributions have been previously observed in larger pores of various materials (55,86–88), and suggest a different translocation mechanism than the main population. Finally, in [Fig. 3 f](#) we plot the fraction of events that fit the model in Eq. 1 for different pore diameters, as obtained by integrating the experimental distributions and the fits. To arrive at these values we converted the dwell time histograms and fits into cumulative distribution functions, and then estimated the percent of excess (i.e., nonfitting) events that lie above the aligned experimental and theoretical cumulative distribution functions. By dividing the area in agreement with this dwell time by the total area of the histogram curve, the percentage of events that agree with our model is determined (see the [Supporting Material SI-4](#) for further discussion). The guideline drawn in [Fig. 3 f](#) (*dashed red line*) shows a plateau of events that fit Eq. 1 for $d = 2.8$ – 3.0 nm (*shaded in green*), whereas a regular emergence of a second process is observed for larger pores. In the optimum regime we can therefore say that the predominant transport mechanism is a smooth 1D first-passage process. Interestingly, for $d = 2.6$ – 2.7 nm ($n = 7$) we find that a significantly lower fraction of events fit the model than for $d = 2.8$ – 2.9 nm ($n = 4$), presumably due to overwhelming DNA/pore interactions.

Next, in [Fig. 4 a](#) we present a compiled set of v and D values for 500 bp DNA transport as a function of pore

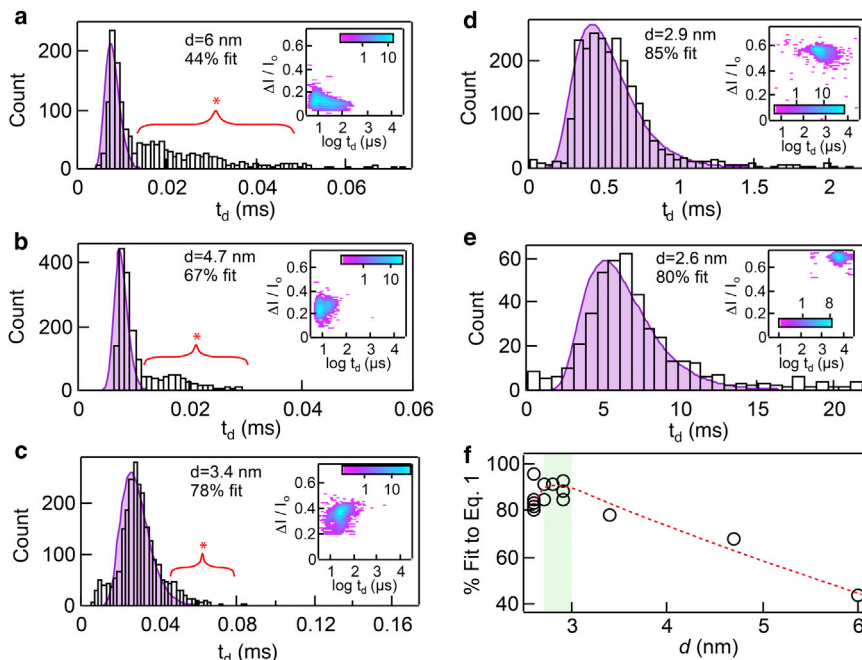


FIGURE 3 The influence of pore diameter on DNA transport time. (*a–e*) Dwell time distributions with drift-diffusion fits included (*shaded purple curves*) for 500 bp DNA translocation through five different pores of diameter d ranging from 2.6 to 6 nm. Our model fits the data by the designated percentages with the shown 2.9 nm pore matching the best, an 85% fit. Pores with $d > 3.4 \text{ nm}$ have distributions with noticeably long tails that lie outside our model curves, as denoted by the red brackets, indicating translocation events with erratic transport through the pore. Insets: Heat maps of fractional current blockade versus the log of the dwell time for each pore diameter. The color scale bars displayed are in log scale. (*f*) By plotting the fit percentages for 14 different pores as a function of d , we see that the optimal pore size for regular DNA transport lies between $d = 2.8$ – 3.0 nm (*green shaded region*). Red dotted line is a guideline for viewing the trend in d . To see this figure in color, go online.

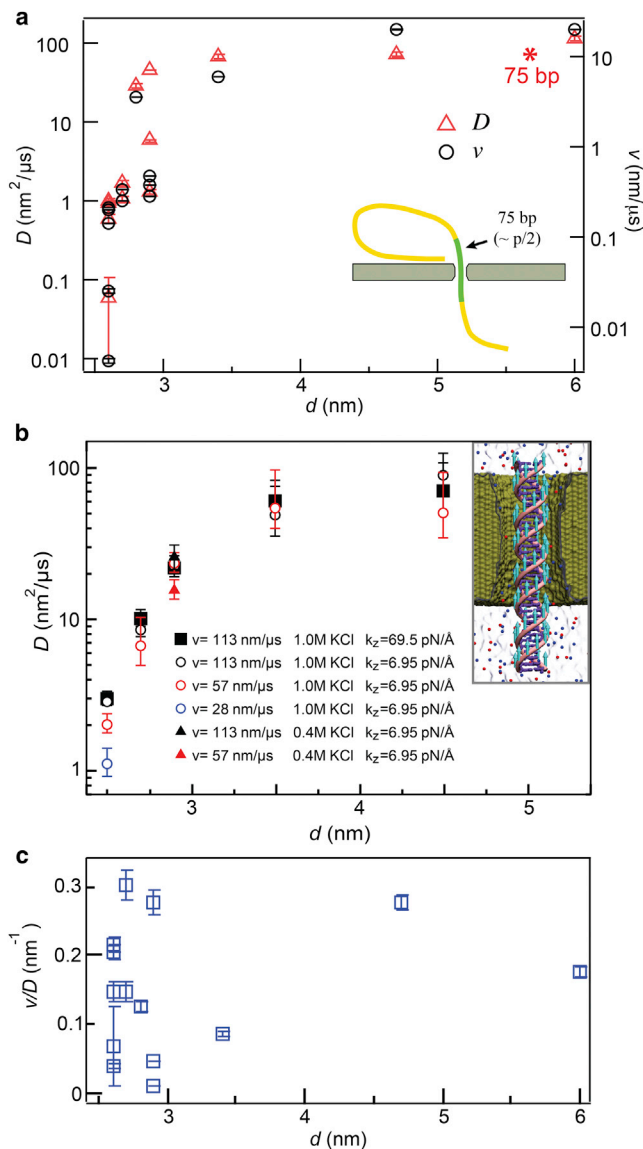


FIGURE 4 Dependence of v and D with respect to pore diameter d . (a) Using our 1D drift-diffusion model, D and v are extracted by fitting our dwell time distributions to Eq. 1. Both parameters increase with d , but asymptotically approach a bulk value once the pore diameter is large enough (> 4 nm). The red asterisk represents the axial diffusion coefficient for the free electrophoresis of a 75 bp DNA molecule ($\sim 68 \text{ nm}^2/\mu\text{s}$) (see the Supporting Material SM-6 for details). (b) MD simulations of DNA diffusion coefficient. The diffusion coefficient was estimated as $k_B Tv/F$, where F was the force required to move DNA with an average velocity v . Each data point represents an average of five independent simulations (except for $d = 4.5$ nm, which is the average of 10 simulations). Estimates of the diffusion coefficient did not depend on the choice of the pulling velocity, stiffness of the pulling restraints, or the ion concentration with the exception of the 2.5 nm diameter nanopore. Inset: Molecular graphics representation of a typical simulation system. A 36 bp fragment of DNA (purple and pink) is pulled through a nanopore in a silicon nitride membrane (green cut-away molecular surface), submerged in solution (gray semitransparent surface) of potassium and chloride ions (blue and red spheres, respectively). Teal arrows illustrate external forces applied to displace DNA with a prescribed translocation velocity v . (c) A plot of our experimental values of v/D as a function of d shows that this ratio remains independent of diameter ($0.15 \pm 0.10 \text{ nm}^{-1}$) for the range $d = 2.6 - 6$ nm. To see this figure in color, go online.

diameter ($n = 14$, effective thickness $b_{\text{eff}} = 7-10$ nm). The trends for both parameters have a striking resemblance: as pore diameter increases from 2.6 to 3.0 nm we observe a drastic increase in both v and D , whereas for $d > 3$ nm both parameters approach asymptotic limits ($v_{\text{max}} \sim 20 \text{ nm}/\mu\text{s}$; $D_{\text{max}} \sim 80 \text{ nm}^2/\mu\text{s}$). Under our experimental conditions, we could not detect 500 bp DNA through $d > 6$ nm pores. To explain the convergence of v and D values for larger pores we turn to the simplistic model of the DNA drift-diffusion problem. By fitting our dwell time distributions to Eq. 1 we seek a solution of first-passage times for rod-like DNA segments to traverse a full DNA contour length through the pore (illustrated in the inset to Fig. 4 a). As argued earlier in the manuscript, for a rod-like DNA length of $\sim 0.5p$ (or 75 bp) we expect an axial diffusion coefficient of $\sim 68 \text{ nm}^2/\mu\text{s}$. As shown by an asterisk in Fig. 4 a, this value is in fair agreement with our observed values of D for $d > 3$ nm ($40-100 \text{ nm}^2/\mu\text{s}$).

In the $d < 3$ nm regime, we find a trend that implies strongly damped DNA diffusion due to confinement. Effects of pore confinement on D are well known (25,89,90), and have been recently observed for protein transport in confining pores (85). We independently assessed the impact of confinement on the diffusion coefficient of dsDNA by employing all-atom MD simulations. Specifically, we constructed five atomic-scale models of the experimental system, each containing a nanopore in a 7-nm-thick silicon nitride membrane, a 36 bp fragment of dsDNA, and an electrolyte solution (see Fig. 4 b). Each nanopore had an hour-glass shape and the nanopore diameters were 2.5, 2.7, 2.9, 3.5, or 4.5 nm. We simulated mechanical pulling of dsDNA through the nanopore (91) while measuring the average force F required to maintain the prescribed translocation velocity v (see Materials and Methods for details). The measured force-velocity dependence was used to estimate the diffusion coefficient via the Einstein relation: $D = k_B Tv/F$. The results of these simulations clearly have a striking, nearly quantitative resemblance to our experimental observations: Simulated D values for pores with $d > 3.5$ nm were quantitatively close to our asymptotic values, whereas in the confined DNA regime systematic decreases in D were observed. Notably, for $d = 2.5$ nm, the diffusion coefficient obtained through the Einstein relation was found to depend on the pulling velocity due to a noticeable friction between the pore wall and the DNA. This is coincidental with our experimental observations, which showed more scatter in D and v values for pores with $d = 2.6-2.7$ nm.

Although the experimental and simulation-based dependence of D on pore size agrees qualitatively (and perhaps semiquantitatively), a comparison of experimental v values in the unconfined regime to values based on free-solution electrophoresis measurements yields a very poor agreement: Stellwagen measured for ~ 75 bp DNA a mobility of $\mu = 3.2 \times 10^{-4} \text{ cm}^2 \text{ V}^{-1} \text{ s}^{-1}$ (84), which, given the electric field in our pores ($E \sim 1.8 \times 10^5 \text{ V/cm}$, corresponding to 200 mV

applied across a 8 nm long nanopore), should yield a drift velocity of ~ 580 nm/ μ s. This is a factor of ~ 26 higher than our largest value of v ($d = 6.0$ nm, $v = 22.5 \pm 0.5$ nm/ μ s). We argue that this discrepancy is an outcome of three major differences from bulk measurements: First, only a fraction (about one-third) of the ~ 75 bp rod-like DNA segment (i.e., a half-persistence length of DNA, or 25 nm) is actually driven by the electric field because our pores are ~ 8 nm thick. Second, in free electrophoresis the electric fields are typically uniform on the scale of a molecule, whereas the large field gradient within a pore cannot act to drive all monomers in the pore equally, further reducing the effective driving force. Finally, dsDNA effective charge is reduced in nanopores to $\sim 0.5 e^-/\text{bp}$ due to electroosmotic effects (one-fourth of formal charge), as determined via single-molecule force measurements (92,93). These combined factors argue for greatly reduced μ values in nanopores, although a quantitative assessment of the reduction requires models that are beyond the scope of this work.

In the more confined regime of $d < 3$ nm we find a sharp and systematic decrease in v values by up to two orders of

magnitude, a trend that remarkably resembles that of D . In Fig. 4 c we compute for the series of 14 pores the ratio v/D . Strikingly, as we found to be voltage-independent in Fig. 2, the parameter v/D remains fairly diameter independent (0.15 ± 0.10 nm $^{-1}$), despite pore-to-pore variance of up to 70%. Given the increased pore-to-pore variance in v/D for sub-3 nm diameter pores, we attribute it to small differences in geometry among the different pores. Therefore, the v/D ratio qualifies as a useful metric when contemplating pore-to-pore variations in experiments.

Mechanism for smooth DNA transport in small pores

We have shown that DNA dwell time distributions of a 500-bp DNA fragment through pores in the regime $d < 3$ nm appear as single populations, whereas in the regime $d = 3.4\text{--}6.0$ nm two populations are observed (Fig. 3). To explain this observed behavior we point to the electric field landscape in the pore vicinity during translocation. In Fig. 5 we present finite element numerical simulations of the electric potential (V) profiles around a $d = 4.0$ nm (Fig. 5, a–c),

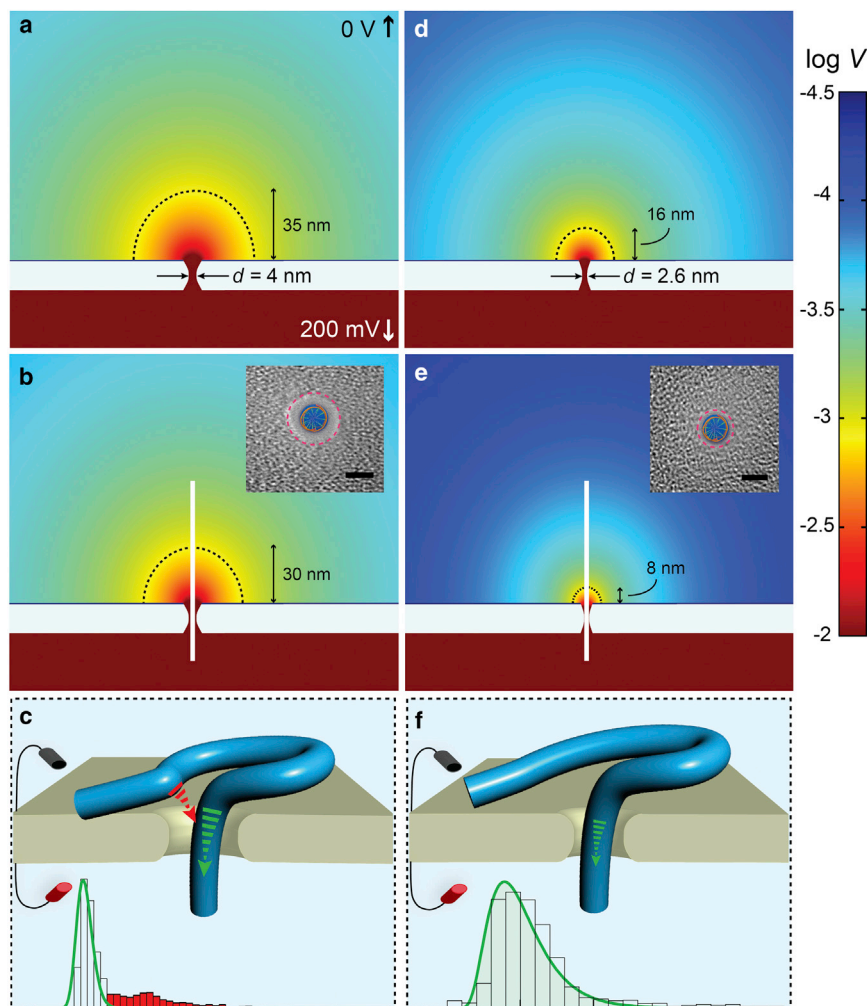


FIGURE 5 Contour plots of $\log V$ from finite element simulations for nanopores of two diameters show the contrast in the residual capture field when DNA threads through the pore (simulation conditions: 200 mV, 0.4 M KCl, 21°C). When the nanopore is open (a and d) there is a wider capture radius for the 4.0 nm pore than for the 2.6 nm pore. Once DNA is threading through the nanopore (b and e) there is a reduction in the electric field, but still enough residual remaining to affect the DNA coil outside the nanopore. Because the DNA occupies a larger percentage of the pore's volume when the diameter is 2.6 nm, its residual field is reduced more significantly ($\sim 50\%$) than in the case of a 4.0 nm diameter ($\sim 14\%$). The dotted black line in each panel indicates where the electric potential is 1 mV. Insets: Transmission electron microscopy images of SiN_x nanopores with dsDNA overlaid to show the occupied area during translocation (scale bar is 2 nm). (c and f) These panels illustrate the effect of coil interference in the case of each diameter. Sample dwell time distributions taken from Fig. 3, b and e, are displayed below to show the added longer dwell times (red-shaded region) that are the result of DNA self-interaction during translocation. To see this figure in color, go online.

and $d = 2.6$ nm pore (Fig. 5, *d–f*) (93–98). Correspondingly, below the open pores we show V profiles for DNA-occupied pores (see the Supporting Material SM-7 for simulation details). We refer the reader to two key observations: 1) the external field above the pore mouth is more pronounced for the larger pore, and 2) DNA threading results in a reduction of this external field in both cases, although this diminution is greater for the small pore. The previous two observations are trivial from experiments, because larger ion currents are observed for larger pores, and larger fractional blockades are seen for smaller pores, respectively. However, this also demands that the impact of the external electric field on the extra-pore DNA segments during its transport is not equal for different pore diameters. For the 2.5 nm pore much of the external field upon DNA threading is self-extinguished, whereas for the 4.0 nm pore DNA causes only a mild reduction. To orient the reader we show using dashed semicircles the 1 mV equipotential lines for all simulations in the figure. For the 4.0 nm pore, the 1 mV contour line is found at a reduced distance from the pore by 14% upon DNA threading, whereas for the 2.6 nm pore the reduction is 50%. As a DNA molecule travels through a larger pore, an extra-pore DNA region of the currently translocating molecule is more likely to be voltage-driven toward the mouth of the larger pore, causing self-interference that stochastically slows/stops the DNA, as observed by the smeared dwell time distribution at longer timescales than predicted by the drift-diffusion model (see Fig. 5 *c*). In contrast, this self-interference is inhibited in the regime $d = 2.8–3.0$ nm, yielding smooth transport (see Fig. 5 *f*). We note that the illustrations in Fig. 5, *c* and *f*, are not to scale, and the pseudo-loop that the DNA forms re-

quires several persistence lengths. As we have shown here, a 500 bp DNA length is sufficient to yield complicated translocation dynamics unless the pore size is restricted to a sub-3 nm diameter.

Smooth transport of long DNA

In Fig. 6 *a* we show representative sets of concatenated events for the different DNA lengths (see Fig. S6 for more traces). Clearly, the events uniformly increase in duration for longer DNA molecules, yet the current blockades remain constant (see Fig. S7) in contrast with a prior report in which DNA length dependence on the conductance blockade fraction was observed for DNA lengths above 2 kbp (55). In Fig. 6 *b* we present log dwell time distributions for transport of 11 DNA lengths in the range 35–20,000 bp through nanopores with $d = 2.8–3.0$ nm. The distributions are represented as color maps, where increasing color intensity represents more populated bins ($n > 280$ for each length shown, see Table S1). Remarkably, we observe a uniform increase in the peak dwell time position with increasing DNA lengths, with the exception of DNA lengths in the range 6–20 kbp, for which there is a significant scattered trail of events with shorter dwell times. After having confirmed using gel electrophoresis that our long DNA fragments are not contaminated with shorter DNA fragments (see Fig. S5), we believe that transport of DNA fragments longer than 6 kbp often involves other processes that are a result of the coil size (e.g., DNA shearing, DNA escape, etc.). However, because this only occurs for a minor fraction of the events, the analytical power of small pores is not entirely limited to DNA lengths below 6 kbp. After having extracted peak

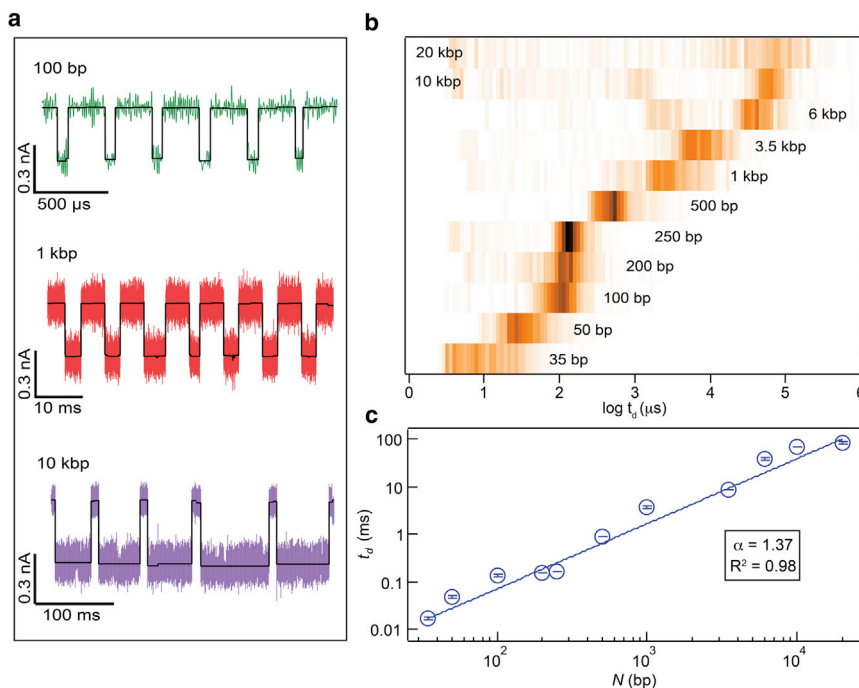


FIGURE 6 Scaling of transport time t_d as a function of DNA length N . (a) Sample concatenated traces of consecutive events for 100 bp, 1 kbp, and 10 kbp with included analysis fits (black solid lines). (b) The normalized dwell time histograms for $N = 35$ bp–20 kbp in 2.9 ± 0.1 nm SiN nanopores (200 mV, pH 7.9, 25°C). Notably, each DNA length < 6 kbp has only one event population in contrast to past results with small nanopores. (c) A logarithmic plot of $\langle t_d \rangle$ vs. N for DNA translocation through pores with $d = 2.9 \pm 0.1$ nm. By fitting our data using a power-law function ($t_d \sim N^\alpha$) for 35 bp $< N < 20,000$ bp we extract a power exponent $\alpha = 1.37$. To see this figure in color, go online.

dwell times from curve fitting the data for each DNA length, we plot the characteristic dwell time t_d vs. N in the regime $35 < N < 20,000$ bp (see Fig. 6 c). The uncertainty in dwell time displayed for each data point is the standard error of the mean (see Table S1). Fitting the results to a power law (i.e., $t_d \sim N^\alpha$) we obtain an exponent of $\alpha = 1.37$ with a Pearson's chi-squared of $R^2 = 0.98$. Power laws such as this have been previously obtained using Monte Carlo simulations (99,100) as well as Langevin and MD simulations (101–104) for dsDNA transport through synthetic pores, although quite a broad range of power laws has been suggested (105). However, the similarity among different reports is striking: experimental studies using $d \sim 10$ nm pores obtained similar values of $\alpha = 1.27$ (16) and $\alpha = 1.34$ (17) to our results, and similarly, for $d = 4$ nm, $\alpha = 1.4$ was found for short DNA fragments (55). In contrast with the latter cited power law, in our experiments we have found a single power-law relationship for the entire DNA length range tested. This power law further suggests a single transport process that does not suffer from stalling mechanisms due to DNA coil self-interference. Reducing the pore diameter to the 2.8–3.0 nm regime helps to eliminate adverse and anomalous motions of DNA transport. However, a standing question that remains is: why is a scaling of $\alpha = 1.3$ –1.4 for dsDNA transport so persistent for such a wide range of nanopore diameters and experimental conditions? Although there are two distinct power-law regimes that are expected,

namely, a scale-free mean velocity (i.e., $\alpha = 1$) in the limit of strongly interacting pores (106) and a parabolic dependence ($\alpha = 2$ –2.5) in the diffusive regime (bias-free escape) (107,108), power laws that are pore diameter-independent imply that for voltage-driven dsDNA translocations hydrodynamic interactions play a pronounced role.

Single-pulse discrimination of DNA lengths

As a demonstration of the high resolution of our nanopores regarding DNA contour length, we used a pore of $d = 2.6$ nm and $b_{eff} = 6$ nm to differentiate between two short DNA lengths: 100 and 500 bp. Upon the addition of a mixture of 100 and 500 bp (1:1 ratio, 30 nM of each length) to the *cis* chamber, it was apparent in real time that two dwell time populations existed as highlighted by asterisks in Fig. 7 a. When binning the transport time data, as shown in Fig. 7 b, we clearly observe two distinct populations for 100 and 500 bp with an overlap of $< 3\%$. The calculated mean dwell times of 190 and 970 μ s correspond well to the values displayed in Fig. 6 c for pores with $d = 2.8$ –3.0 nm, which is due to the use of a thinner pore (6 nm in this case, as compared to 8 nm previously). As an additional confirmation of identifying the correct DNA lengths, we ran the same DNA samples individually in pores of identical dimensions to see if we would obtain similar values for dwell time (t_d). As illustrated in the inset of Fig. 7 b, we found that

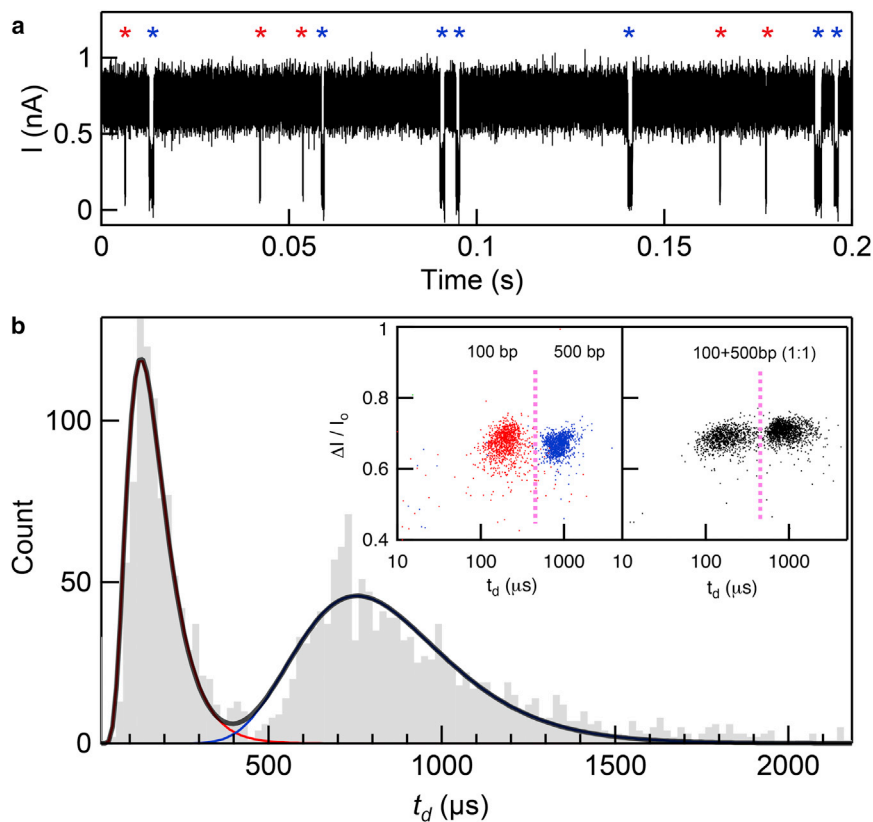


FIGURE 7 Single-pulse discrimination between two DNA fragments. (a) A continuous current trace for a 60 nM equimolar mixture of 100 and 500 bp in a small, thin nanopore (i.e., $d = 2.6$ nm, $b_{eff} = 6$ nm) shows a clear distinction between the two different lengths as denoted by the red and blue asterisks (100 and 500 bp). (b) Dwell time distributions of translocation data from panel a show distinct peaks for 100 and 500 bp. Inset: Scatter plots of the fractional current blockade versus dwell time for the translocation of 100 bp (red) and 500 bp (blue) separately and together in an equimolar mixture (black) in pores of comparable size ($d = 2.6$ nm). Using pores of this size, we are able to distinguish between 100 and 500 bp events with an accuracy of 98.4% and 97.6%, respectively, when dividing the populations at 450 μ s (pink dotted line). In the 60 nM mixture, we determine there are 955 and 1347 translocation events for 100 and 500 bp, respectively. To see this figure in color, go online.

100 and 500 bp samples yielded highly distinguishable populations with $\langle t_d \rangle$ of 210 and 880 μs , respectively. When we set a threshold dwell time of 450 μs (pink dotted line), we find that 98.4% of 100 bp events fall below this limit, whereas 97.6% of 500 bp events lie above this cutoff, demonstrating a $\sim 98\%$ accuracy in differentiating these DNA lengths. When evaluating the relative capture rate in this mixture we find that the capture rate for 500 bp is 68% greater than for 100 bp. This too is in agreement with past results stating that in the presence of an energy barrier for capture due to a small pore, the larger DNA is more likely to be captured (95).

CONCLUSION

We have identified here an optimum pore geometry that leads to smooth transport of double-stranded DNA. The DNA trajectory statistics can be well modeled by first-passage time distributions derived from a 1D drift-diffusion model. The model we have used describes the biased escape of a particle from a trajectory under subjection to a uniform field. Clearly, this 1D model is not sufficiently elaborate for describing a complex process such as semiflexible polymer translocation through thin pores (i.e., nonuniform fields), and other models that capture various phenomena such as polymer-pore interactions and coil effect should be developed and/or implemented to better explain our data. However, we have found that this simple two-parameter model adequately explains our results by providing for each experiment a characteristic axial diffusion coefficient and velocity. Quantitative fits of our data to this model using a bootstrapping algorithm shed light on the DNA translocation process through small pores, and we found that transport through nanopores with $d \sim 3$ nm is smooth, i.e., governed by a drift-diffusion process. Experiments using larger pores in the range 3.4–6.0 nm reveal an additional population with longer dwell times than predicted by the model, which we attribute to DNA coil self-interference that is driven by the external field in larger pores.

We caution the reader that our use of smooth to describe the translocation process does not imply that DNA velocity is constant. For both a single molecule and an ensemble of molecules, translocation velocities are not generally uniform but subject to various types of random forces that overall prescribe normally distributed velocity profiles. We show that the electrophoretic mobility of DNA is smaller than DNA mobility in bulk solution and is a function of applied voltage and pore diameter. Turning to the diameter dependence, experiments and simulations reveal that axial DNA diffusion in small pores is greatly reduced due to confinement, and that this reduced diffusion proportionally reduces the mean velocities to values that are below 0.34 nm/ μs (i.e., v/D is constant). The dependence of translocation time on DNA length reveal a power-law scaling with an exponent of 1.37, in good agreement with other experimental results

using a range of pore diameters. However, for DNA lengths longer than 6 kbp we have found noticeable (though not major) fractions of observed events with shorter dwell times than the major population, which point to coil-induced complications in the transport process. Fine-tuning our pores for smooth DNA transport enabled us to discriminate between 100 and 500 bp in a mixture from individual pulses with $>98\%$ accuracy. This regulation of double-helical DNA transport through nanopores provides a steady control that could prove useful in detecting other structures such as noncanonical DNA motifs, DNA-protein interactions, and epigenetic modifications.

SUPPORTING MATERIAL

Eight figures, one table, and supporting data are available at [http://www.biophysj.org/biophysj/supplemental/S0006-3495\(14\)1068-6](http://www.biophysj.org/biophysj/supplemental/S0006-3495(14)1068-6).

The authors thank Michael D. Edge for assistance with bootstrapping, and Andrey Ivankin, Derek Stein, and Murugappan Muthukumar for helpful discussions.

This work was supported by grants from the National Institutes of Health (R21-HG006873 and R01-HG006321, M.W.; R01-HG007406; NSF DMR-0955959 A.A. and J.W.). The authors gladly acknowledge supercomputer time provided through XSEDE Allocation Grant MCA05S028 and the Blue Waters petascale supercomputer system (UIUC).

SUPPORTING CITATIONS

References (109–115) appear in the Supporting Material.

REFERENCES

1. Kasianowicz, J. J., E. Brandin, ..., D. W. Deamer. 1996. Characterization of individual polynucleotide molecules using a membrane channel. *Proc. Natl. Acad. Sci. USA.* 93:13770–13773.
2. Dekker, C. 2007. Solid-state nanopores. *Nat. Nanotechnol.* 2: 209–215.
3. Branton, D., D. W. Deamer, ..., J. A. Schloss. 2008. The potential and challenges of nanopore sequencing. *Nat. Biotechnol.* 26:1146–1153.
4. Kasianowicz, J. J., J. W. F. Robertson, ..., V. M. Stanford. 2008. Nanoscopic porous sensors. *Annu. Rev. Anal. Chem. (Palo Alto Calif.)*. 1:737–766.
5. Venkatesan, B. M., and R. Bashir. 2011. Nanopore sensors for nucleic acid analysis. *Nat. Nanotechnol.* 6:615–624.
6. Wallace, E. V. B., D. Stoddart, ..., H. Bayley. 2010. Identification of epigenetic DNA modifications with a protein nanopore. *Chem. Commun. (Camb.)*. 46:8195–8197.
7. Wanunu, M., D. Cohen-Karni, ..., M. Drndic. 2011. Discrimination of methylcytosine from hydroxymethylcytosine in DNA molecules. *J. Am. Chem. Soc.* 133:486–492.
8. Shim, J., G. I. Humphreys, ..., R. Bashir. 2013. Detection and quantification of methylation in DNA using solid-state nanopores. *Sci. Rep.* 3:1389.
9. Schreiber, J., Z. L. Wescoe, ..., M. Akeson. 2013. Error rates for nanopore discrimination among cytosine, methylcytosine, and hydroxymethylcytosine along individual DNA strands. *Proc. Natl. Acad. Sci. USA.* 110:18910–18915.
10. Laszlo, A. H., I. M. Derrington, ..., J. H. Gundlach. 2013. Detection and mapping of 5-methylcytosine and 5-hydroxymethylcytosine with nanopore MspA. *Proc. Natl. Acad. Sci. USA.* 110:18904–18909.

11. Akeson, M., D. Branton, ..., D. W. Deamer. 1999. Microsecond time-scale discrimination among polycytidylic acid, polyadenylic acid, and polyuridylic acid as homopolymers or as segments within single RNA molecules. *Biophys. J.* 77:3227–3233.
12. Meller, A., L. Nivon, ..., D. Branton. 2000. Rapid nanopore discrimination between single polynucleotide molecules. *Proc. Natl. Acad. Sci. USA.* 97:1079–1084.
13. Meller, A., and D. Branton. 2002. Single molecule measurements of DNA transport through a nanopore. *Electrophoresis.* 23:2583–2591.
14. Clarke, J., H. C. Wu, ..., H. Bayley. 2009. Continuous base identification for single-molecule nanopore DNA sequencing. *Nat. Nanotechnol.* 4:265–270.
15. Venta, K., G. Shemer, ..., M. Drndić. 2013. Differentiation of short, single-stranded DNA homopolymers in solid-state nanopores. *ACS Nano.* 7:4629–4636.
16. Storm, A. J., C. Storm, ..., C. Dekker. 2005. Fast DNA translocation through a solid-state nanopore. *Nano Lett.* 5:1193–1197.
17. Fologea, D., E. Brandin, ..., J. Li. 2007. DNA conformation and base number simultaneously determined in a nanopore. *Electrophoresis.* 28:3186–3192.
18. Shim, J. W., Q. Tan, and L.-Q. Gu. 2009. Single-molecule detection of folding and unfolding of the G-quadruplex aptamer in a nanopore nanocavity. *Nucleic Acids Res.* 37:972–982.
19. Li, J., M. Gershow, ..., J. A. Golovchenko. 2003. DNA molecules and configurations in a solid-state nanopore microscope. *Nat. Mater.* 2:611–615.
20. Aksimentiev, A., J. B. Heng, ..., K. Schulten. 2004. Microscopic Kinetics of DNA Translocation through synthetic nanopores. *Biophys. J.* 87:2086–2097.
21. Mathé, J., A. Aksimentiev, ..., A. Meller. 2005. Orientation discrimination of single-stranded DNA inside the alpha-hemolysin membrane channel. *Proc. Natl. Acad. Sci. USA.* 102:12377–12382.
22. Michalet, X., A. N. Kapanidis, ..., S. Weiss. 2003. The power and prospects of fluorescence microscopies and spectroscopies. *Annu. Rev. Biophys. Biomol. Struct.* 32:161–182.
23. Levy-Sakin, M., and Y. Eberstein. 2013. Beyond sequencing: optical mapping of DNA in the age of nanotechnology and nanoscopy. *Curr. Opin. Biotechnol.* 24:690–698.
24. Zirkin, S., S. Fishman, ..., Y. Eberstein. 2014. Lighting up individual DNA damage sites by in vitro repair synthesis. *J. Am. Chem. Soc.* 136:7771–7776.
25. Lu, B., F. Albertorio, ..., J. A. Golovchenko. 2011. Origins and consequences of velocity fluctuations during DNA passage through a nanopore. *Biophys. J.* 101:70–79.
26. Thompson, J. F., and J. S. Oliver. 2012. Mapping and sequencing DNA using nanopores and nanodetectors. *Electrophoresis.* 33:3429–3436.
27. Olasagasti, F., K. R. Lieberman, ..., M. Akeson. 2010. Replication of individual DNA molecules under electronic control using a protein nanopore. *Nat. Nanotechnol.* 5:798–806.
28. Lieberman, K. R., G. M. Cherf, ..., M. Akeson. 2010. Processive replication of single DNA molecules in a nanopore catalyzed by phi29 DNA polymerase. *J. Am. Chem. Soc.* 132:17961–17972.
29. Cherf, G. M., K. R. Lieberman, ..., M. Akeson. 2012. Automated forward and reverse ratcheting of DNA in a nanopore at 5-Å precision. *Nat. Biotechnol.* 30:344–348.
30. Manrao, E. A., I. M. Derrington, ..., J. H. Gundlach. 2012. Reading DNA at single-nucleotide resolution with a mutant MspA nanopore and phi29 DNA polymerase. *Nat. Biotechnol.* 30:349–353.
31. Laszlo, A. H., I. M. Derrington, ..., J. H. Gundlach. 2014. Decoding long nanopore sequencing reads of natural DNA. *Nat. Biotechnol.* 32:829–833.
32. Storm, A. J., J. H. Chen, ..., C. Dekker. 2005. Translocation of double-strand DNA through a silicon oxide nanopore. *Phys. Rev. E Stat. Nonlin. Soft Matter Phys.* 71:051903.
33. Mihovilovic, M., N. Hagerty, and D. Stein. 2013. Statistics of DNA capture by a solid-state nanopore. *Phys. Rev. Lett.* 110:028102.
34. Smeets, R. M. M., S. W. Kowalczyk, ..., C. Dekker. 2009. Translocation of RecA-coated double-stranded DNA through solid-state nanopores. *Nano Lett.* 9:3089–3096.
35. Venkatesan, B. M., D. Estrada, ..., R. Bashir. 2012. Stacked graphene-Al2O3 nanopore sensors for sensitive detection of DNA and DNA-protein complexes. *ACS Nano.* 6:441–450.
36. Jin, Q., A. M. Fleming, ..., H. S. White. 2013. Structural destabilization of DNA duplexes containing single-base lesions investigated by nanopore measurements. *Biochemistry.* 52:7870–7877.
37. Wanunu, M., J. Sutin, and A. Meller. 2009. DNA profiling using solid-state nanopores: detection of DNA-binding molecules. *Nano Lett.* 9:3498–3502.
38. Singer, A., M. Wanunu, ..., A. Meller. 2010. Nanopore based sequence specific detection of duplex DNA for genomic profiling. *Nano Lett.* 10:738–742.
39. Kowalczyk, S. W., A. R. Hall, and C. Dekker. 2010. Detection of local protein structures along DNA using solid-state nanopores. *Nano Lett.* 10:324–328.
40. Carlsen, A. T., O. K. Zahid, ..., A. R. Hall. 2014. Selective detection and quantification of modified DNA with solid-state nanopores. *Nano Lett.* 14:5488–5492.
41. Fologea, D., J. Uplinger, ..., J. Li. 2005. Slowing DNA translocation in a solid-state nanopore. *Nano Lett.* 5:1734–1737.
42. Li, J., and D. S. Talaga. 2010. The distribution of DNA translocation times in solid-state nanopores. *J. Phys. Condens. Matter.* 22:454129.
43. Kowalczyk, S. W., D. B. Wells, ..., C. Dekker. 2012. Slowing down DNA translocation through a nanopore in lithium chloride. *Nano Lett.* 12:1038–1044.
44. Uplinger, J., B. Thomas, ..., J. Li. 2012. K(+), Na(+), and Mg(2+) on DNA translocation in silicon nitride nanopores. *Electrophoresis.* 33:3448–3457.
45. Venkatesan, B. M., B. Dorvel, ..., R. Bashir. 2009. Highly sensitive, mechanically stable nanopore sensors for DNA analysis. *Adv. Mater.* 21:2771–2776.
46. Larkin, J., R. Henley, ..., M. Wanunu. 2013. Slow DNA transport through nanopores in hafnium oxide membranes. *ACS Nano.* 7:10121–10128.
47. Lu, B., D. P. Hoogerheide, ..., J. A. Golovchenko. 2013. Pressure-controlled motion of single polymers through solid-state nanopores. *Nano Lett.* 13:3048–3052.
48. Zhang, H., Q. Zhao, ..., D. Yu. 2013. Slowing down DNA translocation through solid-state nanopores by pressure. *Small.* 9:4112–4117.
49. Kim, Y. R., J. Min, ..., C. Ko. 2007. Nanopore sensor for fast label-free detection of short double-stranded DNAs. *Biosens. Bioelectron.* 22:2926–2931.
50. Wanunu, M., and A. Meller. 2007. Chemically modified solid-state nanopores. *Nano Lett.* 7:1580–1585.
51. Anderson, B. N., M. Muthukumar, and A. Meller. 2013. pH tuning of DNA translocation time through organically functionalized nanopores. *ACS Nano.* 7:1408–1414.
52. Wang, D., S. Harrer, ..., A. Afzali-Ardakani. 2014. Regulating the transport of DNA through biofriendly nanochannels in a thin solid membrane. *Sci. Rep.* 4:3985.
53. Squires, A. H., J. S. Hersey, ..., A. Meller. 2013. A nanopore-nanofiber mesh biosensor to control DNA translocation. *J. Am. Chem. Soc.* 135:16304–16307.
54. Heng, J. B., C. Ho, ..., G. Timp. 2004. Sizing DNA using a nanometer-diameter pore. *Biophys. J.* 87:2905–2911.
55. Wanunu, M., J. Sutin, ..., A. Meller. 2008. DNA translocation governed by interactions with solid-state nanopores. *Biophys. J.* 95:4716–4725.

56. Briggs, K., H. Kwok, and V. Tabard-Cossa. 2014. Automated fabrication of 2-nm solid-state nanopores for nucleic acid analysis. *Small*. 10:2077–2086.
57. van den Hout, M., V. Krudde, ..., N. H. Dekker. 2010. Distinguishable populations report on the interactions of single DNA molecules with solid-state nanopores. *Biophys. J.* 99:3840–3848.
58. Carlsen, A. T., O. K. Zahid, ..., A. R. Hall. 2014. Interpreting the conductance blockades of DNA translocations through solid-state nanopores. *ACS Nano*. 8:4754–4760.
59. Raillon, C., P. Granjon, ..., A. Radenovic. 2012. Fast and automatic processing of multi-level events in nanopore translocation experiments. *Nanoscale*. 4:4916–4924.
60. Phillips, J. C., R. Braun, ..., K. Schulten. 2005. Scalable molecular dynamics with NAMD. *J. Comput. Chem.* 26:1781–1802.
61. Darden, T., D. York, and L. Pedersen. 1993. Particle mesh Ewald: An N.log(N) method for Ewald sums in large systems. *J. Chem. Phys.* 98:10089–10092.
62. Batcho, P. F., D. A. Case, and T. Schlick. 2001. Optimized particle-mesh Ewald/multiple-time step integration for molecular dynamics simulations. *J. Chem. Phys.* 115:4003–4018.
63. Andersen, H. C. 1983. RATTLE: A “Velocity” version of the SHAKE algorithm for molecular dynamics calculations. *J. Comput. Phys.* 52:24–34.
64. Miyamoto, S., and P. A. Kollman. 1992. SETTLE: an analytical version of the SHAKE and RATTLE algorithm for rigid water models. *J. Comput. Chem.* 13:952–962.
65. MacKerell, A. D., D. Bashford, ..., M. Karplus. 1998. All-atom empirical potential for molecular modeling and dynamics studies of proteins. *J. Phys. Chem. B*. 102:3586–3616.
66. Yoo, J., and A. Aksimentiev. 2012. Improved parameterization of Li⁺, Na⁺, K⁺, and Mg²⁺ ions for all-atom molecular dynamics simulations of nucleic acid systems. *J. Phys. Chem. Lett.* 3:45–50.
67. Heng, J. B., A. Aksimentiev, ..., G. Timp. 2006. The electromechanics of DNA in a synthetic nanopore. *Biophys. J.* 90:1098–1106.
68. Martyna, G. J., D. J. Tobias, and M. L. Klein. 1994. Constant pressure molecular dynamics algorithms. *J. Chem. Phys.* 101:4177–4189.
69. Shore, D., J. Langowski, and R. L. Baldwin. 1981. DNA flexibility studied by covalent closure of short fragments into circles. *Proc. Natl. Acad. Sci. USA*. 78:4833–4837.
70. Muthukumar, M. 2011. Polymer Translocation. CRC Press, Boca Raton, FL.
71. Ling, D. Y., and X. S. Ling. 2013. On the distribution of DNA translocation times in solid-state nanopores: an analysis using Schrödinger’s first-passage-time theory. *J. Phys. Condens. Matter*. 25:375102.
72. Zhou, Z., Y. Hu, ..., X. Lu. 2013. DNA translocation through hydrophilic nanopore in hexagonal boron nitride. *Sci. Rep.* 3:3287.
73. Wanunu, M., T. Dadosh, ..., M. Drndić. 2010. Rapid electronic detection of probe-specific microRNAs using thin nanopore sensors. *Nat. Nanotechnol.* 5:807–814.
74. Kowalczyk, S. W., A. Y. Grosberg, ..., C. Dekker. 2011. Modeling the conductance and DNA blockade of solid-state nanopores. *Nanotechnology*. 22:315101.
75. Chen, P., J. Gu, ..., D. Branton. 2004. Probing single DNA molecule transport using fabricated nanopores. *Nano Lett.* 4:2293–2298.
76. Nkodo, A. E., J. M. Garnier, ..., G. W. Slater. 2001. Diffusion coefficient of DNA molecules during free solution electrophoresis. *Electrophoresis*. 22:2424–2432.
77. Stellwagen, E., and N. C. Stellwagen. 2002. Determining the electrophoretic mobility and translational diffusion coefficients of DNA molecules in free solution. *Electrophoresis*. 23:2794–2803.
78. McMullen, A., H. W. de Haan, ..., D. Stein. 2014. Stiff filamentous virus translocations through solid-state nanopores. *Nat. Commun.* 5:4171.
79. Wang, L., and H. Yu. 1988. Chain conformation of linear polyelectrolyte in salt solutions: sodium poly(styrenesulfonate) in potassium chloride and sodium chloride. *Macromolecules*. 21:3498–3501.
80. Nicolai, T., and M. Mandel. 1989. Dynamic light scattering by aqueous solutions of low-molar-mass DNA fragments in the presence of sodium chloride. *Macromolecules*. 22:2348–2356.
81. Goinga, H. T., and R. Pecora. 1991. Dynamics of low molecular weight DNA fragments in dilute and semidilute solutions. *Macromolecules*. 24:6128–6138.
82. Maier, B., and J. O. Rädler. 1999. Conformation and self-diffusion of single DNA molecules confined to two dimensions. *Phys. Rev. Lett.* 82:1911.
83. Stellwagen, N. C., S. Magnusdottir, ..., P. G. Righetti. 2001. Measuring the translational diffusion coefficients of small DNA molecules by capillary electrophoresis. *Biopolymers*. 58:390–397.
84. Stellwagen, E., Y. Lu, and N. C. Stellwagen. 2003. Unified description of electrophoresis and diffusion for DNA and other polyions. *Biochemistry*. 42:11745–11750.
85. Larkin, J., R. Y. Henley, ..., M. Wanunu. 2014. High-bandwidth protein analysis using solid-state nanopores. *Biophys. J.* 106:696–704.
86. Soni, G. V., A. Singer, ..., A. Meller. 2010. Synchronous optical and electrical detection of biomolecules traversing through solid-state nanopores. *Rev. Sci. Instrum.* 81:014301.
87. Merchant, C. A., K. Healy, ..., M. Drndić. 2010. DNA translocation through graphene nanopores. *Nano Lett.* 10:2915–2921.
88. Venkatesan, B. M., A. B. Shah, ..., R. Bashir. 2010. DNA sensing using nano-crystalline surface enhanced Al(2)O(3) nanopore sensors. *Adv. Funct. Mater.* 20:1266–1275.
89. Renkin, E. M. 1954. Filtration, diffusion, and molecular sieving through porous cellulose membranes. *J. Gen. Physiol.* 38:225–243.
90. Hoogerheide, D. P., F. Albertorio, and J. A. Golovchenko. 2013. Escape of DNA from a weakly biased thin nanopore: experimental evidence for a universal diffusive behavior. *Phys. Rev. Lett.* 111:248301.
91. Aksimentiev, A. 2010. Deciphering ionic current signatures of DNA transport through a nanopore. *Nanoscale*. 2:468–483.
92. Keyser, U. F., B. N. Koeleman, ..., C. Dekker. 2006. Direct force measurements on DNA in a solid-state nanopore. *Nat. Phys.* 2:473–477.
93. van Dorp, S., U. F. Keyser, ..., S. G. Lemay. 2009. Origin of the electrophoretic force on DNA in solid-state nanopores. *Nat. Phys.* 5:347–351.
94. Liu, H., S. Qian, and H. H. Bau. 2007. The effect of translocating cylindrical particles on the ionic current through a nanopore. *Biophys. J.* 92:1164–1177.
95. Wanunu, M., W. Morrison, ..., A. Meller. 2010. Electrostatic focusing of unlabelled DNA into nanoscale pores using a salt gradient. *Nat. Nanotechnol.* 5:160–165.
96. He, Y., M. Tsutsui, ..., T. Kawai. 2011. Gate manipulation of DNA capture into nanopores. *ACS Nano*. 5:8391–8397.
97. Lu, B., D. P. Hoogerheide, ..., D. Yu. 2012. Effective driving force applied on DNA inside a solid-state nanopore. *Phys. Rev. E Stat. Nonlin. Soft Matter Phys.* 86:011921.
98. He, Y., M. Tsutsui, ..., T. Kawai. 2013. Mechanism of how salt-gradient-induced charges affect the translocation of DNA molecules through a nanopore. *Biophys. J.* 105:776–782.
99. Dubbeldam, J. L. A., A. Milchev, ..., T. A. Vilgis. 2007. Driven polymer translocation through a nanopore: a manifestation of anomalous diffusion. *Europhys. Lett.* 79:18002.
100. Vocks, H., D. Panja, ..., R. C. Ball. 2008. Pore-blockade times for field-driven polymer translocation. *J. Phys. Condens. Matter*. 20:095224.
101. Luo, K., S. T. T. Ollila, ..., A. Bhattacharya. 2008. Dynamical scaling exponents for polymer translocation through a nanopore. *Phys. Rev. E Stat. Nonlin. Soft Matter Phys.* 78:050901.
102. Fyta, M., S. Melchionna, ..., E. Kaxiras. 2008. Hydrodynamic correlations in the translocation of a biopolymer through a nanopore: theory

- and multiscale simulations. *Phys. Rev. E Stat. Nonlin. Soft Matter Phys.* 78:036704.
103. Izmitli, A., D. C. Schwartz, ..., J. J. de Pablo. 2008. The effect of hydrodynamic interactions on the dynamics of DNA translocation through pores. *J. Chem. Phys.* 128:085102.
104. Bhattacharya, A., W. H. Morrison, ..., K. Binder. 2009. Scaling exponents of forced polymer translocation through a nanopore. *Eur. Phys. J. E Soft Matter* 29:423–429.
105. Panja, D., G. T. Barkema, and A. B. Kolomeisky. 2013. Through the eye of the needle: recent advances in understanding biopolymer translocation. *J. Phys. Condens. Matter* 25:413101.
106. Lubensky, D. K., and D. R. Nelson. 1999. Driven polymer translocation through a narrow pore. *Biophys. J.* 77:1824–1838.
107. Muthukumar, M. 1999. Polymer translocation through a hole. *J. Chem. Phys.* 111:10371–10374.
108. Chuang, J., Y. Kantor, and M. Kardar. 2002. Anomalous dynamics of translocation. *Phys. Rev. E Stat. Nonlin. Soft Matter Phys.* 65:011802.
109. Kim, M. J., M. Wanunu, ..., A. Meller. 2006. Rapid fabrication of uniformly sized nanopores and nanopore arrays for parallel DNA analysis. *Adv. Mater.* 18:3149–3155.
110. Kim, M. J., B. McNally, ..., A. Meller. 2007. Characteristics of solid-state nanometre pores fabricated using a transmission electron microscope. *Nanotechnology* 18:205302.
111. Smeets, R. M. M., U. F. Keyser, ..., C. Dekker. 2008. Noise in solid-state nanopores. *Proc. Natl. Acad. Sci. USA* 105:417–421.
112. Tabard-Cossa, V., D. Trivedi, ..., A. Marziali. 2007. Noise analysis and reduction in solid-state nanopores. *Nanotechnology* 18:305505.
113. Hall, J. E. 1975. Access resistance of a small circular pore. *J. Gen. Physiol.* 66:531–532.
114. Vodyanoy, I., and S. M. Bezrukov. 1992. Sizing of an ion pore by access resistance measurements. *Biophys. J.* 62:10–11.
115. Li, G., and J. X. Tang. 2004. Diffusion of actin filaments within a thin layer between two walls. *Phys. Rev. E Stat. Nonlin. Soft Matter Phys.* 69:061921.

Supporting Material

Smooth DNA Transport Through a Narrowed Pore Geometry

Spencer Carson¹, Jim Wilson², Aleksei Aksimentiev², and Meni Wanunu^{1,3†}

[†]Email: wanunu@neu.edu

SM-1: Materials and Methods.....	2
SM-2: Effect of low-pass filter frequencies on event detection.....	3
SM-3: Time stability and pore-to-pore reproducibility of DNA translocation	5
SM-4: Determination of pore diameter and thickness based on open and blocked pore ionic current (I_o and I_b)	6
SM-5: Determination of fit percentage using the 1D drift-diffusion model	7
SM-6: Derivation of axial diffusion coefficient D_A	7
SM-7: Finite element simulations of DNA nanopore translocation	8
SM-8: Agarose gel of DNA samples.....	10
SM-9: Transport time vs. DNA length studies	11
Supporting References.....	15

SM-1: *Materials and Methods*

Nanopore experiments. Substrates for our solid-state nanopore membranes were formed by the thermal oxidation of silicon <100> wafers to generate a $\sim 2.5\text{-}\mu\text{m}$ thick SiO_2 dielectric barrier layer. Following oxidation, low-pressure chemical vapor deposition is used to deposit a 45-nm-thick low-stress silicon nitride layer. Using a combination of photolithography and dry/wet etching steps, a wafer was etched to obtain an array of $5\times 5\text{ mm}^2$ chips with freestanding square membranes at their centers (10-50 μm in length), and further thinned to $\sim 25\text{ nm}$ using a controlled reactive ion etch process. A transmission electron microscope (JEOL 2010FEG) at high energy (200 kV) and magnification (1.5 Mx) was then used to “drill” nanopores of measureable shape and diameters in the range of 2-10 nm. Due to various factors we have found that our effective nanopore diameters did not always correspond to the TEM-based diameter, so all quoted pore diameters in the paper were estimated from ion current measurements using a solitary model in which the effective thickness is 1/3 of the total membrane thickness (see SM-4).(1, 2)

Prior to conducting a nanopore experiment the nanopore chips were cleaned by a 10-minute immersion in a fresh heated piranha solution (1:2 mixture of H_2O_2 and H_2SO_4), followed by cooling and a copious rinse with water. The chips were then stored in DI water until an experiment was carried out. Upon use, the chips were vacuum dried and mounted on a gasket-sealed two-chamber cell, each equipped with an electrode that is connected to a high-bandwidth amplifier. Buffered electrolyte (0.4 M KCl, buffered to pH 7.9 using 10 mM Tris and 1 mM EDTA) was added to both chambers, and the pore was evaluated by conductance measurements and by recording a time-stable DC ion current response for nonzero bias.

Molecular dynamics simulations. A custom telforces script was used to produce DNA displacement. Each phosphorous atom of DNA was harmonically restrained ($k_z = 69.5$ or $6.9\text{ pN}/\text{\AA}$) to an individual template particle. The z coordinates of the template particles were synchronously changed according to the target DNA velocity. The initial coordinates of the template particles were that of B-form DNA. In addition to the above pulling restraints, the phosphorous atoms of the DNA were harmonically restrained ($k_{rad} = 69.5\text{ pN}/\text{\AA}$) to a cylindrical

shell coaxial with the pore. Under such restraints, the DNA fragment could rotate about its axis but not stretch or move away from the center of the pore. In each production simulation, the DNA was pulled 3.4 nm through the nanopore. Three pulling velocities were used: 0.1133 nm/ns, 0.0567 nm/ns, and 0.0283 nm/ns, requiring 30, 60, and 120 ns simulation, respectively. Five independent simulations were carried out for each pulling velocity; five additional simulations were done for the 4.5 nm nanopore, where thermal fluctuations were more significant. The instantaneous force applied to all phosphorous atoms was recorded every 200 fs. The time average of the instantaneous force was used to determine the diffusion constant.

Bootstrapping and fit optimization. We estimated D and v using a numerical maximum-likelihood procedure. We first eliminated any dwell time data points that were caused by fast collision events or falsely detected by our analysis software by setting a minimum and maximum threshold for dwell time. After these limits were incorporated, standard errors for D and v were estimated by bootstrapping. For each experimental dataset, we created 10,000 bootstrap samples by resampling from the original data with replacement. The estimates of D and v generated from these resampled datasets formed bootstrap distributions for D and v . The distributions were approximately Gaussian, so we report the standard deviation of each bootstrap distribution as a standard error for the corresponding parameter estimate.

SM-2: Effect of low-pass filter frequencies on event detection

Many nanopore experiments are conducted with high salt conditions (i.e., > 1 M KCl or other electrolytic salt), which boosts the ionic current and reduces the relative amplitude of thermal and capacitive noise.(3, 4) Since our experiments use an ionic concentration of 0.4 M KCl we need to take great care in deciding what low-pass filter to apply when analyzing our experimental data. Many factors, such as desired time resolution and signal noise, must be taken into consideration when determining what filtering should be done on nanopore current traces. The low-pass filter selected can also change the number and types of events detected based on the current amplitude ΔI of each respective event. As a demonstration of this effect, in **Fig. S1** we have plotted a sample 2-second current trace from an experiment for 100 bp after applying a filter of 10 kHz (*black*) and 200 kHz (*green*). All translocation events, signified by deeper current blockades, are detected for both filters, but a few collision events are only detected by the 10 kHz filter (*designated by red ovals*).

Since these collisions are masked by the noise when filtering at 200 kHz, we effectively sift out undesirable events by simply increasing our filter frequency without the need of additional manual analysis.

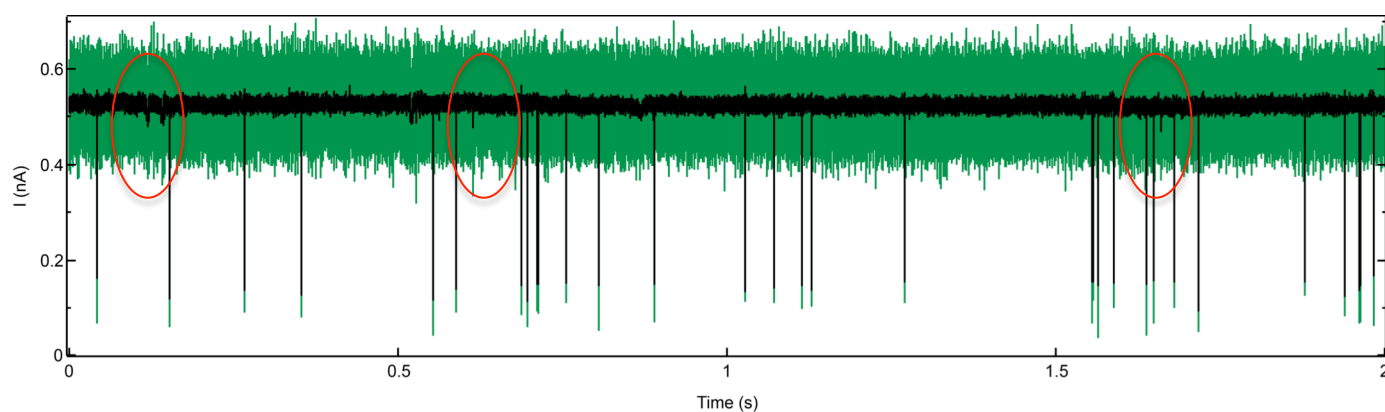


FIGURE S1 Effect of signal bandwidth on masking DNA collision spikes. A two-second example current trace for 100 bp DNA ($V = 200$ mV, $d = 2.9$ nm) is low-pass filtered to 10 kHz (*black*) and 200 kHz (*green*). As seen by the red ovals, collisions of DNA with the pore, which yielded low-amplitude spikes, are missed by our event analysis routine, which was performed on data low-pass filtered at 200 kHz.

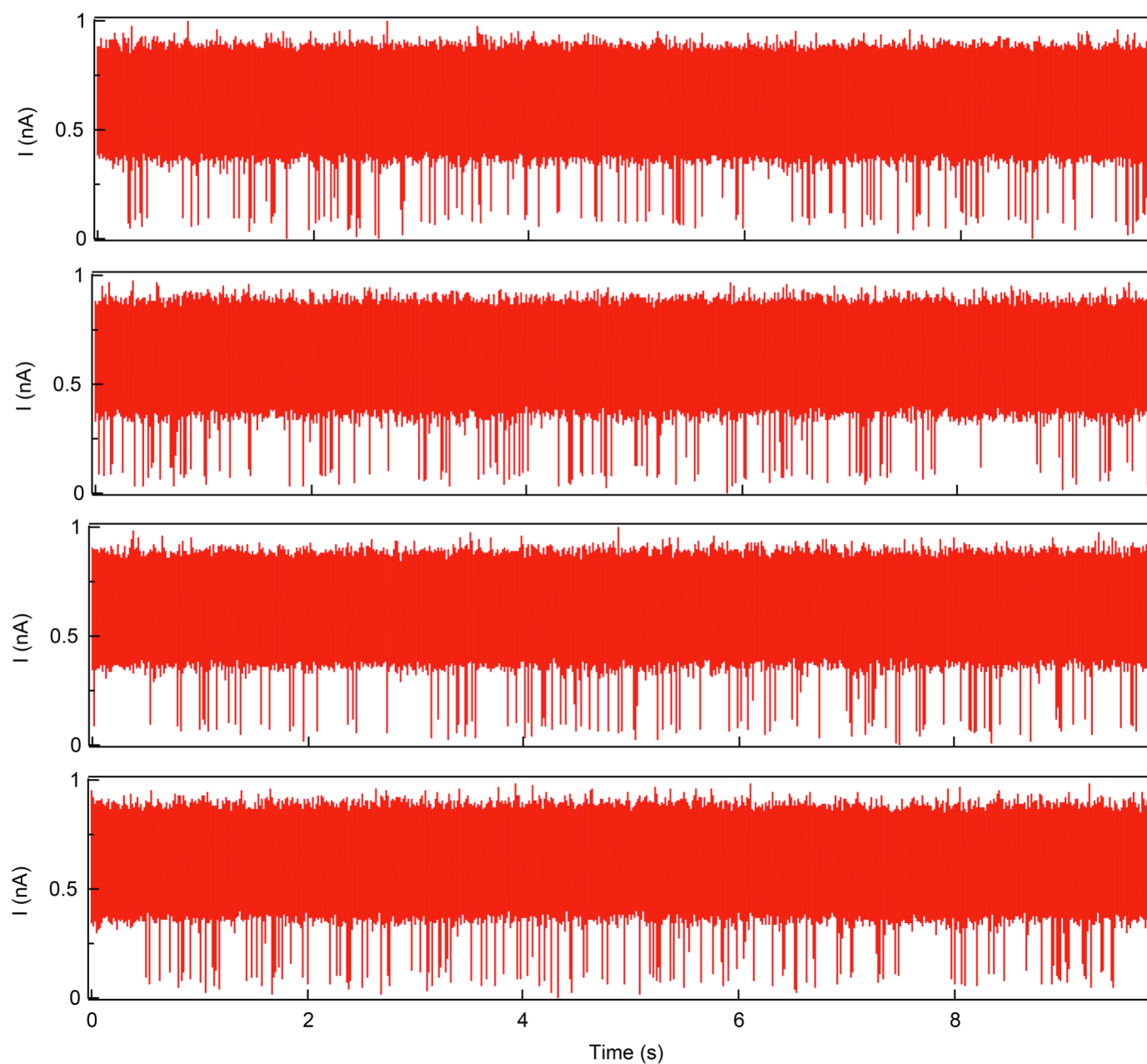
SM-3: Time stability and pore-to-pore reproducibility of DNA translocation

FIGURE S2 A representative, continuous 40-second current trace for 500 bp transport at $V = 200$ mV through a pore of $d = 3.0$ nm (raw data downsampled to 500 kHz and low-pass filtered at 200 kHz). The vast majority of events show great uniformity in both dwell time t_d and current blockade ΔI .

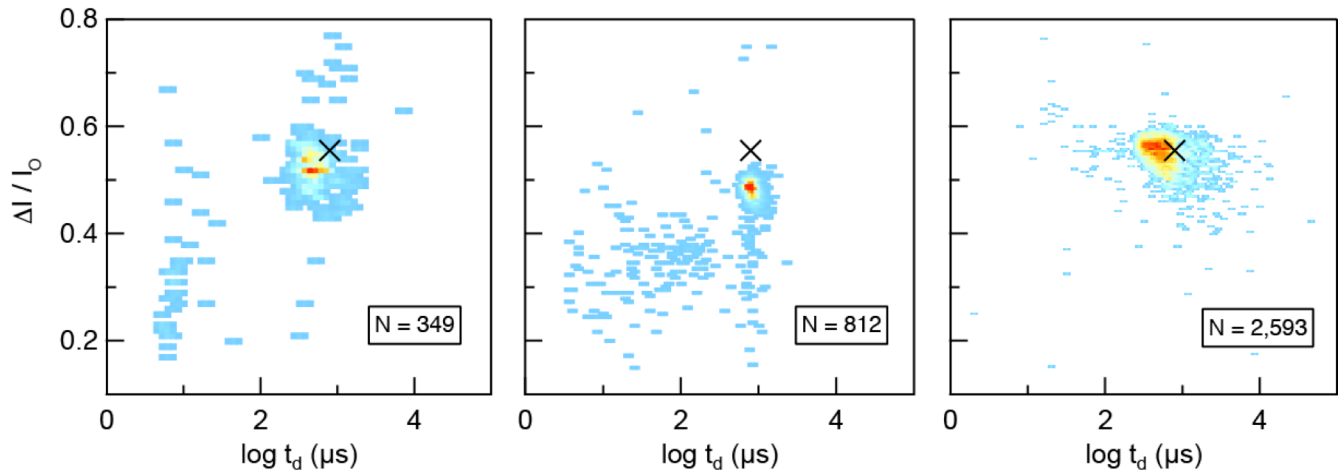


FIGURE S3 Contour plots of 500 bp DNA translocation at $V = 200$ mV for three different pores with $d = 2.8 - 3.0$ nm and similar thickness ($b_{\text{eff}} = 8 - 10$ nm). Each experiment yielded a mean dwell time in the range of 600-900 μs , demonstrating nice reproducibility in our nanopores. The X marker on each plot designates the mean dwell time and fractional current blockade of the dataset with the greatest number of events (*right panel*).

SM-4: Determination of pore diameter and thickness based on open and blocked pore ionic current (I_o and I_b)

To estimate the size any nanopore (diameter and thickness), we used the following nanopore conductance model:(5)

$$I = \sigma V \left(\frac{4b_{\text{eff}}}{\pi d^2} + \frac{1}{d} \right)^{-1} \quad (\text{S1})$$

The first term inside the parentheses represents the classical geometrical contribution to the resistance due to the length and diameter of the nanopore ($R \sim b_{\text{eff}}/d^2$). The second term is known as the access resistance, which dominates as $b_{\text{eff}} \rightarrow 0$ and prevents the resistance from becoming zero in this limit.(6, 7) We first analyzed our current traces to determine the open pore current I_o and the blocked pore current I_b for a given pore. With these two quantities, along with the known applied

voltage V and the solution conductance σ (~50 mS/cm for 0.4 M KCl), it is possible to solve this conductance model numerically to estimate the pore diameter d and the effective membrane thickness b_{eff} for any experiment. Since the nanopores that we fabricated by TEM drilling are hourglass shaped, it has been determined experimentally that it is most accurate to model the membrane using one-third of the total thickness, also known as the effective thickness b_{eff} . (1, 2) Fitting our current data to this model also served as a useful confirmation of the diameter we estimated from our TEM images. Any pore diameter cited in this paper is the value determined experimentally using Eq. S1.

SM-5: Determination of fit percentage using the 1D drift-diffusion model

When using the 1D drift-diffusion model described in the main text, we constrained the fit to a specific thickness b , which was calculated using **Eq. S1** and the known DNA length ($b = b_{eff} + L_C$). Using this thickness constraint we obtained values for D and v when fitting our model to each dwell time distribution. The percentage of dwell time data that is beneath the fitting function was determined by an integration method, which estimates what fraction of our data is contained by the fit. This method was assisted by using an automated integration function in Igor Pro (WaveMetrics, Inc., Portland, OR), which computes the cumulative area integral of both the dwell time histogram and the fitting function over the entire time range of the data. By aligning these two cumulative area curves on the same plot, the percentage of events that agree with our model can be determined. This is accomplished by finding the dwell time where the experimental curve deviates from the fit curve, then dividing the area corresponding to this dwell time by the total area of the experimental histogram, which yields a fractional value representing the fit percentage. When using this method we also made certain to exclude events that occur at fast time scales outside of the fit.

SM-6: Derivation of axial diffusion coefficient D_A

When extracting diffusion coefficients from our dwell time distributions, we relate this to a bulk value of D_o for 75 bp, or one-half of a persistence length for dsDNA. Approximating DNA as a short rod-like molecule, the bulk diffusion coefficient D_o can be broken down into its axial and radial components, D_A and D_R . Since our model is one-dimensional and we are interested in the DNA

translocation trajectory, only the axial component of the diffusion D_A is relevant. By ignoring end-effects of the molecule, the axial component can be approximated as $D_A \sim 2D_R$.⁽⁸⁾ Using this relationship and the fact that $D_o = (D_A + 2D_R)/3$,⁽⁹⁾ we solve for D_A to obtain $D_A = 3/2 D_o$. For notational simplicity, D_A is referred to as D in the main article.

SM-7: Finite-element simulations of DNA nanopore translocation

As shown in **Fig. S4**, we modeled our experimental setup as two cylindrical compartments, each with a diameter of $12\ \mu\text{m}$ and a height of $10\ \mu\text{m}$, connected by an hourglass shaped nanopore. By defining our geometry in this way, we have assumed that our membrane is a perfect electrical insulator, which is an acceptable simplification for materials such as SiN_x . The two important user-defined parameters for the nanopore geometry are the diameter d and the effective membrane thickness b_{eff} , which defines the total membrane thickness (i.e., $3b_{\text{eff}}$) and is used to construct the hourglass shape of the pore. The diameter of the pore opening was defined as $2.5d$, which yielded an

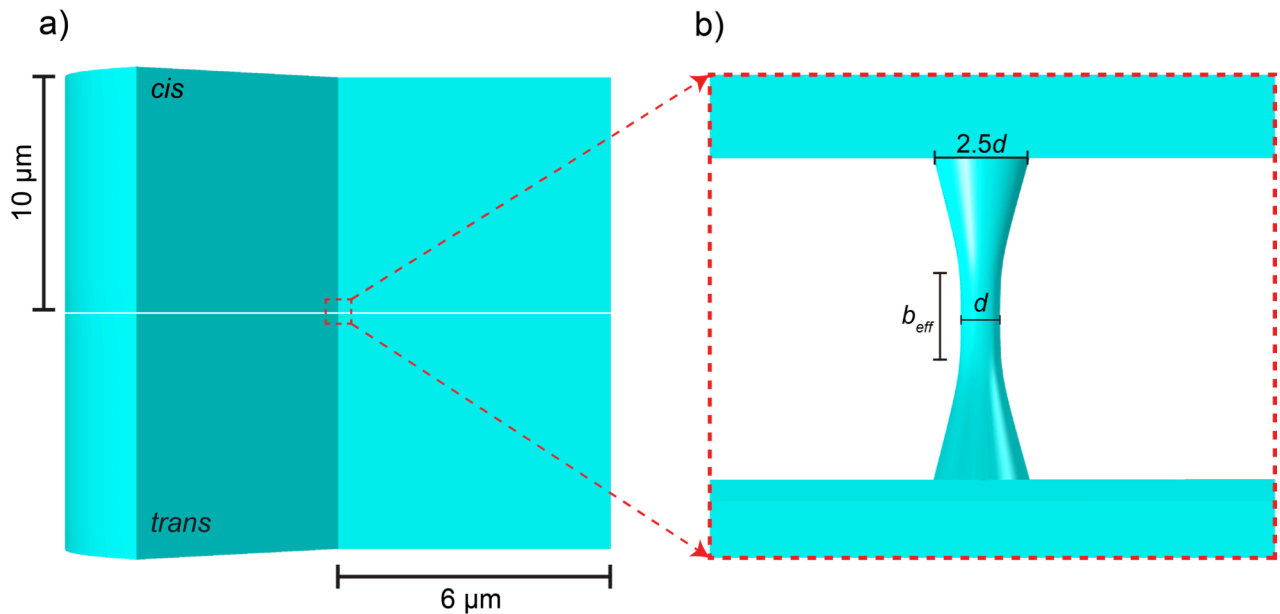


FIGURE S4 Finite element simulation details. **(a)** An illustration of our custom simulation geometry with two cylindrical compartments (*cis* and *trans*) connected by a nanoscale pore. **(b)** An enlarged view of the hourglass-shaped nanopore that joins the two chambers across an insulating membrane (*white region*). The notable variables of diameter d and effective pore length b_{eff} are the most crucial when defining our pore geometry. As noted in the main text, b_{eff} is simply taken to be one-third of the total membrane thickness.

hourglass shape reasonably consistent with TEM imaging previously reported.(2) Whenever DNA was added to the geometry of the simulation (**Fig. 5, b** and **d**) it was modeled as an insulating cylinder with a diameter of 2.2 nm and height of 80 nm. We defined our mesh to be much finer inside and in the vicinity of the nanopore (meshing elements as small as 0.1 nm), and then used normal meshing settings for the rest of the geometry (elements > 1 nm). We also added boundary layers to our mesh at the edges of the nanopore, which will dampen any adverse effects of the sharp edges at the pore/compartment interface. In order to reduce the simulation time, all simulations were computed in two dimensions with a symmetry axis centered inside the pore and perpendicular to the membrane surface. Any results reported were obtained using a temperature of 21°C, a KCl concentration of 0.4 M, and an applied voltage of 200 mV.

All results were steady-state solutions of the Poisson-Nernst-Planck equations, which involve three different physics models in COMSOL. The first and simplest model to implement is the Poisson equation,

$$\nabla^2 V = \frac{-\rho}{\epsilon_0 \epsilon_r} \quad (\text{S2})$$

with ϵ_r as the relative permittivity of water (which we take to be 80) and ρ as the summed charge density of K^+ and Cl^- ions. This equation couples V with the concentration of ions C_i since the space charge density is $\rho = F(C_K - C_{Cl})$, where F is the Faraday constant. The boundary condition used in this model is a zero charge on all surfaces with the exception of setting $V = 0$ V at the top of the *cis* compartment and $V = 200$ mV at the bottom of the *trans* compartment. The second physics model used is the Navier-Stokes equation,

$$\rho_w (\mathbf{u} \cdot \bar{\nabla}) \mathbf{u} = \eta \bar{\nabla}^2 \mathbf{u} - \bar{\nabla} p + \mathbf{F} \quad (\text{S3})$$

where ρ_w is the density of water, \mathbf{u} is the fluid velocity, η is the viscosity of water, p is the pressure, and \mathbf{F} is the sum of all external forces per unit volume. The only external force that is significant in our experiment is the volume electrostatic force due to ionic charge, $\mathbf{F}(r, z) = -\bar{\nabla} V \cdot F(C_K - C_{Cl})$. A no slip boundary condition was enforced in this model at all surfaces. The final physics model employed is a simplified Nernst-Planck equation,

$$\bar{\nabla} \cdot (D \bar{\nabla} C_i + z_i \mu F C_i \bar{\nabla} V) - \mathbf{u} \cdot \bar{\nabla} C_i = 0 \quad (\text{S4})$$

where D is the diffusion coefficient (which we estimate as $2 \times 10^{-9} \text{ cm}^2/\text{s}$ for K^+ and Cl^-), z_i is the charge number of each ionic species, and μ is the electrophoretic mobility defined using the Einstein-Smoluchowski relation $\mu = D / k_b T$. This equation has been simplified by assuming that our fluid is incompressible ($\bar{\nabla} \cdot \mathbf{u} = 0$) and enforcing a steady-state solution ($\partial C_i / \partial t = 0$). The boundary conditions given for this model are a salt concentration of 0.4 M KCl at the top cap of the *cis* chamber and bottom cap of the *trans* chamber, and no flux of ions at any surface in the geometry. This model incorporates all forms of motion for the ionic species in a nanopore experiment: diffusion, electro-migration, and convection.

SM-8: Agarose gel of DNA samples

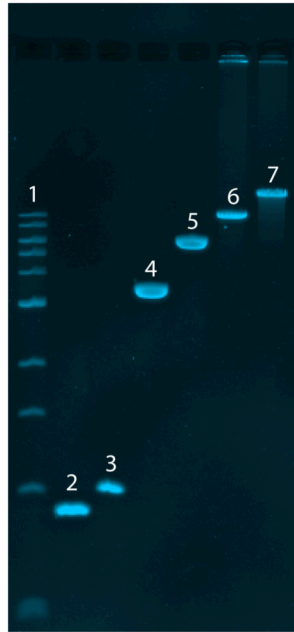


FIGURE S5 An agarose gel of DNA lengths 1 kbp – 20 kbp. To ensure that our long DNA samples ($N > 1$ kbp) are pure, we prepared and a 1% agarose gel with a 1 kb ladder as a control and ran it for 100 minutes at 100 V. After staining the gel with ethidium bromide for ~ 30 min, it was then imaged. Each sample is labeled in the gel as follows: (1) 1 kb ladder, (2) 900 bp (not used in experiments), (3) 1 kbp, (4) 3.5 kbp, (5) 6 kbp, (6) 10 kbp, (7) 20 kbp. As observed in the gel results, each DNA sample shows one clear band that corresponds to the correct length according to the 1 kb ladder.

SM-9: Transport Time vs. DNA Length Studies

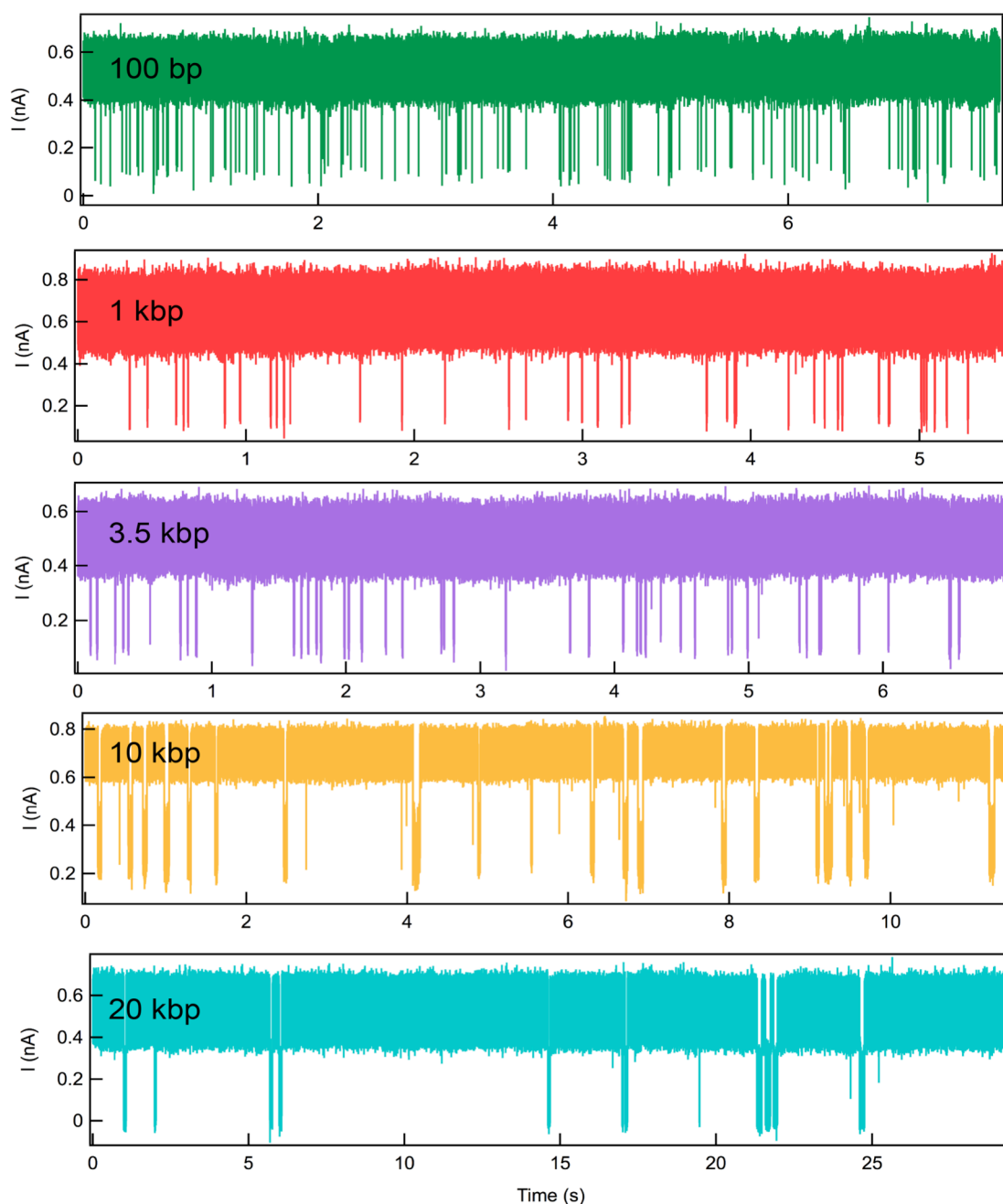


FIGURE S6 Continuous current traces for 100 bp, 1 kbp, 3.5 kbp, 10 kbp and 20 kbp DNA for nanopores with $d = 2.8\text{-}3.0$ nm. The mean open pore current ranges from 0.5-0.7 nA due to small variances in membrane thickness. Despite the open pore current being stable, it would occasionally increase (i.e., $< 10\%$) over the course of an experiment due to solution evaporation or pore expansion, which required the vast majority of datasets to be collected in experiments of less than 20 minutes in duration. Longer DNA lengths had lower sample concentrations to avoid the clogging of our pores due to the longer transport times required for translocation.

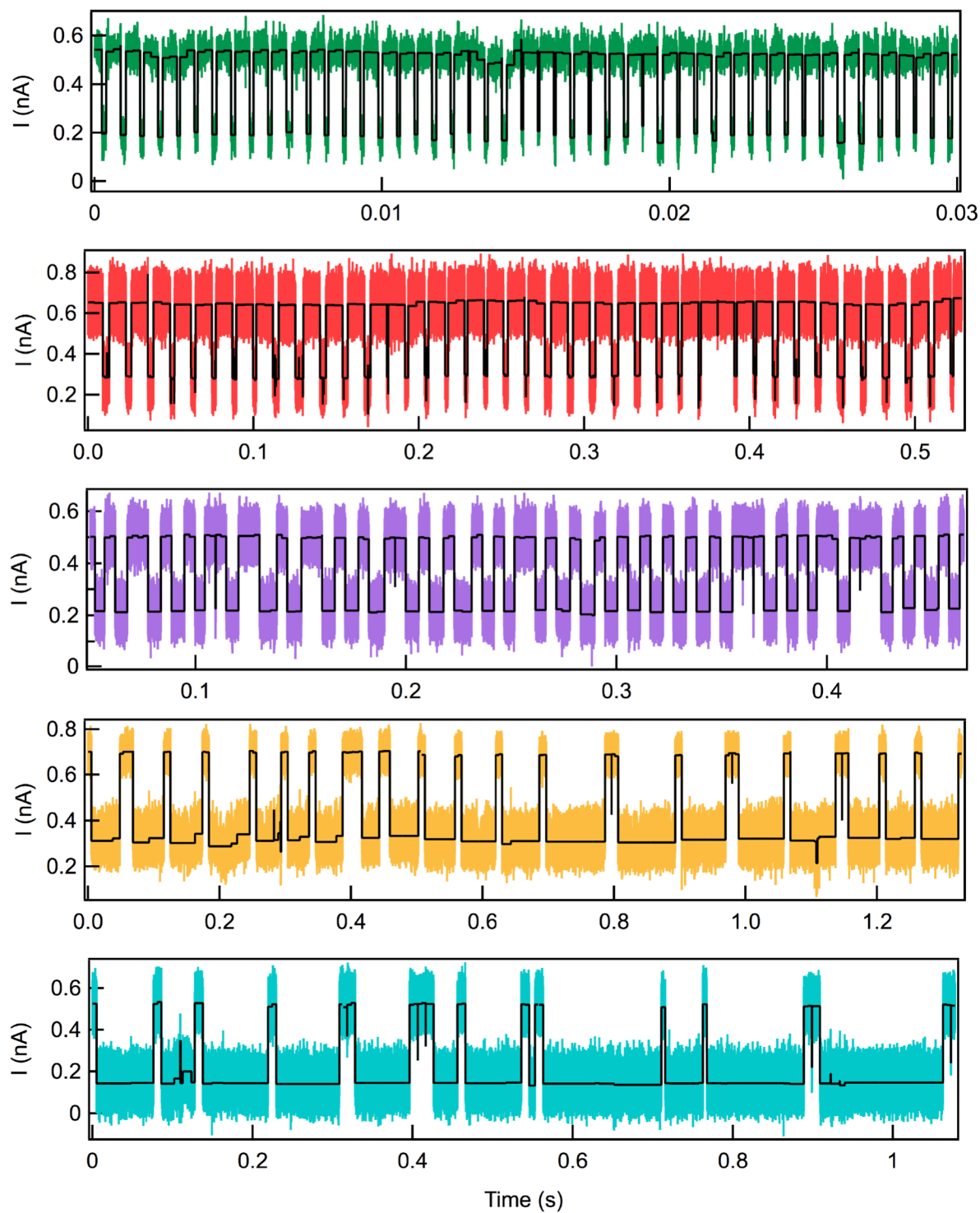


FIGURE S7 Concatenated current traces of consecutive events for the data shown in Figure S6 overlaid with analysis fits obtained by OpenNanopore software. The traces show that we detect a vast majority of translocations with a single current blockade level with the occasional fast collision or multi-level translocation.

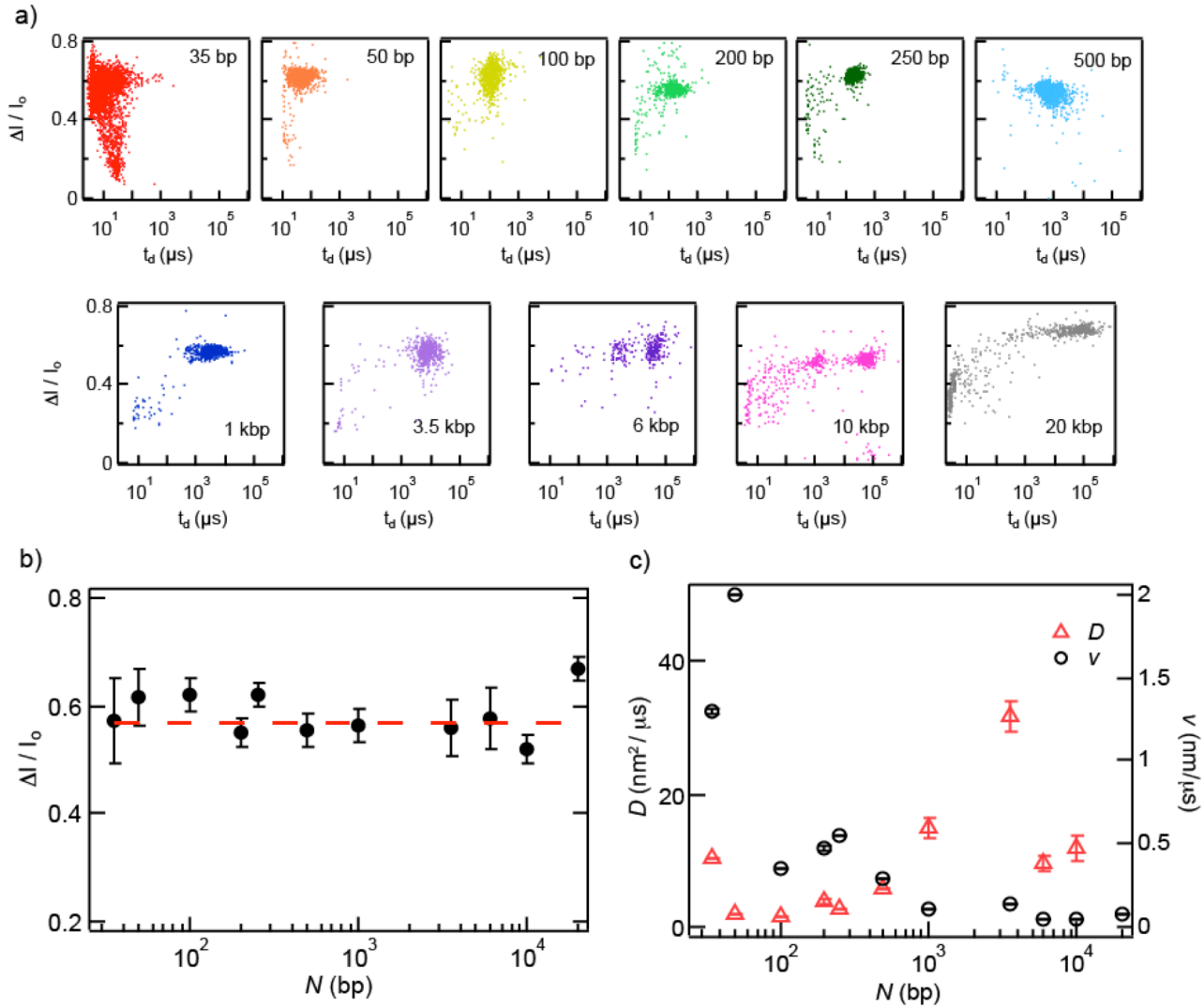


FIGURE S8 (a) Scatter plots of $\Delta I/I_0$ vs. t_d for 11 DNA fragments through different nanopores, all in the range of $d = 2.8\text{-}3.0$ nm. Single event populations are seen for $N < 6$ kbp, while additional populations are seen for DNA lengths $N > 6$ kbp. The fast ($t_d < 100$ μs) events for long DNA are attributed to DNA collisions with the pore, caused by an increased barrier for a long DNA end to find the pore mouth. Further, we speculate that the additional slow population that forms for $N > 6$ kbp is due to DNA shearing or some other disruptive process by the nanopore. Contamination was ruled out by observing a single band in the gel electrophoresis for these fragments (see **Fig. S5**), and we do not have any proof for our claim of DNA shearing (apart from the faster timescale of these events than expected). Since this intermediate population contains a very small minority of the total events, we claim that the slowest population corresponds to DNA translocations. (b) A plot of $\Delta I/I_0$ vs. N for the pores used in (a), demonstrating the similar diameters used in the experiments. When fitting to a horizontal line, we find a mean $\langle \Delta I/I_0 \rangle$ value of 0.57. (c) A plot of v vs. N shows a decreasing velocity with contour length. However, in the plot of D vs. N no definite trend is discernable. The anomalously high value of D for $N = 20$ kbp ($D = 270$ $\text{nm}^2 \mu\text{s}^{-1}$) is not shown in the plot in order to show the trend for most of the other DNA lengths.

TABLE S1. Dwell Time vs. DNA Length Data

<i>N</i> (bp)	<i>n</i>_{total}	<i>t</i>_d (\pm <i>err</i>)
35	3315	$17 \pm 1 \mu\text{s}$
50	2121	$49 \pm 2 \mu\text{s}$
100	911	$135 \pm 8 \mu\text{s}$
200	679	$153 \pm 4 \mu\text{s}$
250	806	$169 \pm 3 \mu\text{s}$
500	2593	$890 \pm 20 \mu\text{s}$
1000	552	$3.62 \pm 0.14 \text{ ms}$
3500	590	$8.51 \pm 0.25 \text{ ms}$
6000	283	$39.1 \pm 2.2 \text{ ms}$
10,000	424	$67 \pm 2 \text{ ms}$
20,000	419	$80 \pm 4 \text{ ms}$

Supporting References

1. Kim, M. J., M. Wanunu, D. C. Bell, and A. Meller. 2006. Rapid fabrication of uniformly sized nanopores and nanopore arrays for parallel DNA analysis. *Adv. Mater.* 18:3149-3155.
2. Kim, M. J., B. McNally, K. Murata, and A. Meller. 2007. Characteristics of solid-state nanometre pores fabricated using a transmission electron microscope. *Nanotechnology.* 18:205302.
3. Smeets, R. M. M., U. F. Keyser, N. H. Dekker, and C. Dekker. 2008. Noise in solid-state nanopores. *P. Natl. Acad. Sci. USA.* 105:417-421.
4. Tabard-Cossa, V., D. Trivedi, M. Wiggin, N. N. Jetha, and A. Marziali. 2007. Noise analysis and reduction in solid-state nanopores. *Nanotechnology.* 18:305505.
5. Wanunu, M., T. Dadosh, V. Ray, J. M. Jin, L. McReynolds, and M. Drndic. 2010. Rapid electronic detection of probe-specific microRNAs using thin nanopore sensors. *Nat. Nanotechnol.* 5:807-814.
6. Hall, J. E. 1975. Access resistance of a small circular pore. *J. Gen. Physiol.* 66:531-532.
7. Vodyanoy, I., and S. M. Bezrukov. 1992. Sizing of an ion pore by access resistance measurements. *Biophys. J.* 62:10-11.
8. Li, G., and J. X. Tang. 2004. Diffusion of actin filaments within a thin layer between two walls. *Phys. Rev. E.* 69:061921.
9. McMullen, A., H. W. de Haan, J. X. Tang, and D. Stein. 2014. Stiff filamentous virus translocations through solid-state nanopores. *Nature Communications.* 5.